ELECTROMAGNETIC LEVITATION OF A SOLID METALLIC TORUS

By

Delbert James Jackson

A thesis submitted in conformity with the requirements
for the degree of Master of Applied Science,
Graduate Department of Metallurgy and Materials Science,
University of Toronto

Electromagnetic Levitation of a Solid Metallic Torus
Master Of Applied Science (2000)
By Delbert James Jackson
Department of Metallurgy and Materials Science
University of Toronto

ABSTRACT

The electromagnetic levitation of a solid metallic torus has been investigated using both experiments and analysis. The investigation was primarily focused on bulk stability and the magnetic pressure distribution on the toroidal surface. Three different induction coil designs were studied: a two-loop design, a reverse-loop design, and a basket design.

The two-loop design did not exhibit bulk stability. The reverse-loop design was shown to exhibit bulk stability, however the magnetic pressure distribution on the surface of the torus is inadequate for levitating large amounts of molten metal. Stable levitation could not be achieved during experiments with the basket design, due to output voltage limitations of the available power supply. The analysis of the basket design showed that it should exhibit bulk stability if properly energized, and that the magnetic pressure distribution is adequate for levitating large amounts of molten metal.

ACKNOWLEDGMENTS

First, I would like to thank Professor Bendzsak for helping me throughout the course of this project. It was a real struggle, but you put your faith in me and encouraged me to do something I didn't think I was capable of doing. Thanks for all the cups of coffee as well. I must thank Professor Perovic and Professor Wang, for helping me to stay focused. Also, thanks to Professor Lavers for answering so many of my questions about electromagnetic fields.

The financial support of ALCAN and the University of Toronto is gratefully acknowledged.

TABLE OF CONTENTS

LIST OF TABLES

LIST OF FIGURES

LIST OF PRINCIPAL SYMBOLS

$\mathbf{A}$	Magnetic vector potential
A_ϕ	Angular component of magnetic vector potential
$\mathbf{B}$	Total magnetic flux density vector
$\mathbf{B_a}$	Applied magnetic flux density vector
B_t	Peak value of magnetic flux density vector component tangent to surface
B_r	Peak radial component of **B**
B_z	Peak axial component of **B**
d	Load displacement from axis of symmetry
f	Excitation frequency
$\mathbf{f_L}$	Lorentz force
$\mathbf{F_b}$	Bulk electromagnetic force
F_z	Bulk electromagnetic lifting force acting on load
F_r	Bulk electromagnetic radial force acting on load
g	Acceleration of gravity
h	Load levitation height
h_s	Separation height between lifting loops and reverse-loop
$\mathbf{I}$	Current phasor
$\mathbf{I_C}$	Coil current phasor
I_o	Magnitude of coil current phasor
$\mathbf{J}$	Current density
j	Imaginary number $(-1)^{1/2}$
$\mathbf{j}$	Surface current density
k	Complete elliptic integral parameter
L	Self Inductance
L_C	Self inductance of the induction coil
M	Mutual inductance
m	Mass of load
$\mathbf{n}$	Normal unit vector
P_M	Time-averaged magnetic pressure
R	Resistance

R_e	Reynolds number
r_a	Mean radius of torus
r_b	Cross-sectional radius of torus
r_s	Radius of a sphere
$\hat{\mathbf{r}}$	Unit radial vector in the cylindrical co-ordinate system
t	Time
u_o	Characteristic velocity of the fluid
V	Voltage
$\mathbf{V}$	Voltage phasor
V_S	Surface flow velocity
$\hat{\mathbf{z}}$	Axial unit vector in the cylindrical co-ordinate system
γ	Surface tension
Γ	Load volume
δ	Electromagnetic penetration depth
θ	Angular co-ordinate
μ_o	Magnetic permeability of a vacuum
ν	Nominal kinematic viscosity
ν_T	Kinematic eddy viscosity
ρ	Density
σ	Electrical conductivity
$\hat{\phi}$	Angular unit vector in the cylindrical co-ordinate system
ψ	Fluid flow streamfunction
ψ_m	Total magnetic flux
ω	Angular excitation frequency
ω_r	Angular frequency of horizontal mechanical oscillation
ω_z	Angular frequency of vertical mechanical oscillation
ω_{res}	Resonant frequency of L-C circuit

CHAPTER 1
INTRODUCTION

1.1 Basic Principle

When a metallic object is placed above an energized induction coil, the time-varying magnetic field generated by the coil induces eddy-currents in the object. The interaction between the induced currents and the applied magnetic field produces an electromagnetic force, called the Lorentz force. The Lorentz force can be used to balance the weight of the object and levitate it. This is the principle of electromagnetic levitation. In addition, the induced currents generate heat in the object, which may be sufficient to melt it. This process is called levitation melting.

1.2 Advantage of Levitation Melting

The levitation melting process is a well-established technique used in chemical and physical metallurgy. It has one main advantage over the traditional process of crucible melting. In levitation melting, the molten metal does not come into contact with a crucible wall. This reduces the amount of contamination. The levitation melting process is advantageous in the manufacture of equipment which require ultra-pure and/or highly reactive metals. Levitation melting is also used to measure surface tension and viscosity of liquid metals and alloys.

1.3 Levitation of a Metallic Sphere

Levitation melting of a metallic spherical load is a typical process that has been achieved many times. A typical induction coil for sphere-levitation is shown in Figure 1-1. A brief description of this system will provide an introduction to the physics of electromagnetic levitation.

The induction coil is a helical conductor that carries an alternating current. The current is generated by a high-frequency power supply, and the excitation frequency f is typically between 10 kHz and 100 kHz. The coil may be approximated by a number of coaxial loops connected in series. The current in each loop can be expressed as a vector using phasor notation:

$$\mathbf{I}_C = \pm I_o e^{j\omega t}\hat{\phi} \qquad (1.1)$$

where I_o is the magnitude of the current phasor (Amperes), j is the imaginary number $\sqrt{-1}$, ω is the angular frequency of the current (radians per second), t is time (seconds), and $\hat{\phi}$ is the angular unit vector in the cylindrical coordinate system. The coil can be divided into two subsections. The lower set of loops is called the lifting coil, as it provides most of the lifting force. The upper set of loops is called the stabilizing coil, because it provides stability and prevents the load from moving in the horizontal direction. The two sets are generally wound such that their currents flow in opposite directions.

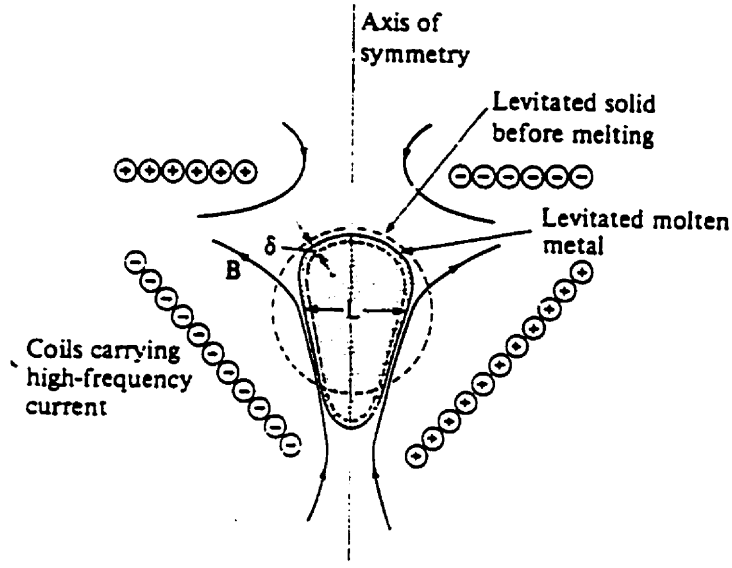

Figure 1-1, Spherical Levitation Device,
from Sneyd et al.[1]

The current-loops of the coil generate a time-varying magnetic field that is essentially axisymmetric. This is specified by the applied magnetic flux density vector $\mathbf{B}_a$. The magnetic flux density is measured in Webers per square meter. For a circular loop carrying a current $\mathbf{I}_C$, $\mathbf{B}_a$ can be determined at any point q in the r-z plane using the Biot-Savart formula:

$$\mathbf{B}_a = \frac{\mu_o}{4\pi}\oint_C \frac{\mathbf{I}_C \times \hat{\mathbf{r}}_q}{r_q^2} dl \qquad (1.2)$$

This formula is a line-integration evaluated on the closed path C of the loop, as shown in Figure 1-2. μ_o is the magnetic permeability of a vacuum ($4\pi x10^{-7}$ H/m), dl is the elemental length of the conductor, r_q is the distance between the point q and dl, and $\hat{\mathbf{r}}_q$ is the unit vector pointing from dl to q. The total applied magnetic field produced by all loops in the coil can be determined using the principle of superposition.

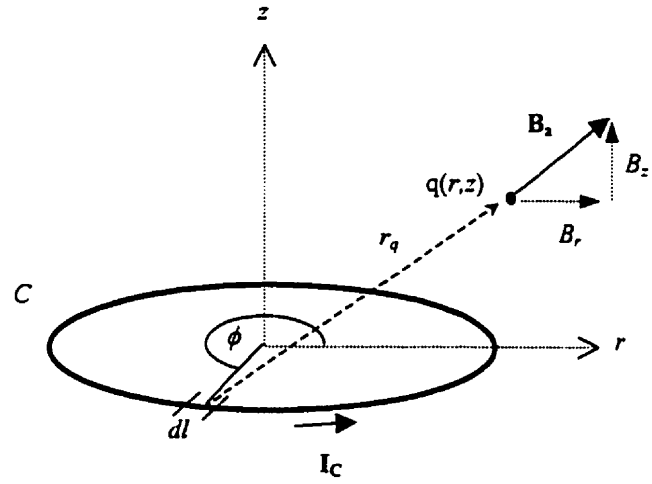

Figure 1-2, Magnetic field produced by a current-carrying loop

The spherical load is situated inside the coil. The load is assumed to be nonmagnetic, meaning that the magnetic permeability of the material μ is the same as that of a vacuum. The electrical conductivity σ and the density ρ are assumed to be constants. The time-varying magnetic field induces eddy-currents in the load. These generally travel in the $\hat{\phi}$ direction, and are specified by the current-density vector **J**. The current density has the units of Amperes per square meter. The eddy-currents also create a magnetic field. The total magnetic field **B** is a superposition of the magnetic fields produced by both the coil currents and the eddy-currents.

The Lorentz force $\mathbf{f}_L$ is generated as a result of the cross-product of the eddy-currents and the applied magnetic flux density. The Lorentz force is measured in N/m^3, and gives the

force acting on an elemental volume dv of the load. Both $\mathbf{J}$ and $\mathbf{B_a}$ oscillate with an angular frequency ω. As a result, the Lorentz force will have both a steady component and an oscillating component with an angular frequency of 2ω. At high frequencies, the oscillating component is negligible, since the response to the cyclical force is limited by the inertia of the load. The expression for the steady component of the Lorentz force is:

$$\mathbf{f}_L = \tfrac{1}{2}\,\mathrm{Re}\left[\mathbf{J} \times \mathbf{B}_a^*\right] \tag{1.3}$$

where $\mathbf{B_a}^*$ is the complex conjugate of $\mathbf{B_a}$. The bulk electromagnetic force $\mathbf{F_b}$ is obtained by integrating the Lorentz force over the entire volume of the load Γ.

$$\mathbf{F}_b = \iiint_{\Gamma} \mathbf{f}_L \cdot dv \tag{1.4}$$

Levitaion may occur when the bulk electromagnetic force is equal and opposite to the weight of the load, or when:

$$\mathbf{F}_b = mg\hat{\mathbf{z}} \tag{1.5}$$

where m is the mass of the sphere (kg) and g is the acceleration of gravity (9.81 m/s^2).

At high frequencies, the induced eddy-currents are confined to a region close to the surface of the load. The penetration depth δ is a parameter used to approximate the depth of this region.

$$\delta = \sqrt{\frac{2}{\omega\mu\sigma}} \tag{1.6}$$

As Figure 1-1 illustrates, the penetration depth is typically much smaller than the characteristic dimension of the load. Beneath the penetration depth, the magnetic field and current-density are practically zero. This phenomenon is sometimes called bulk diamagnetism, as eddy-currents on the surface generate a magnetic field that cancels out the applied magnetic field within the sphere. The load is essentially supported by a magnetic pressure distribution acting on the surface. The time-averaged magnetic pressure P_M, measured in N/m^2, is given by:

$$P_M = \frac{B_t^{\,2}}{4\mu_o} \tag{1.7}$$

where B_t is the peak value of the component of $\mathbf{B}$ tangential to the surface.

The eddy-currents generate heat in the load, which may be sufficient to melt it. Once the load is in the molten state, the surface is free to adjust according to the pressures acting upon it. At every point on the surface, there exists a hydrostatic pressure due to the weight of the liquid metal. The magnetic pressure P_M must balance the hydrostatic pressure at all points if the molten metal is to be properly contained. Figure 1-3 shows the cross-section of the spherical load, assumed to be in the molten state. The location of a point on the surface is specified by the angle θ. The magnetic pressure distribution that balances the hydrostatic pressure distribution is given by the equation:

$$P_M = \rho g r_s (1 - \sin\theta) \qquad (1.8)$$

where ρ is the density of the molten metal (kg/m^3), g is the acceleration of gravity, and r_s is the radius of the sphere (m).

One major problem with this levitation system is that the magnetic pressure distribution does not match the distribution of Equation 1.8. Figure 1-1 indicates a sketch of the magnetic field. At the highest and lowest point on the surface of the load, both the tangential magnetic field and the magnetic pressure are zero. The hydrostatic pressure is greatest at the lowest point and there is no magnetic pressure to balance it. Therefore, when the load melts, the molten metal tends to leak out through the bottom. This is called a 'magnetic hole'. The molten load assumes a distorted 'top' shape as a result of the inadequate pressure distribution. It is only the surface tension that can prevent leakage from occurring. For this reason, the mass of molten metal that can be suspended with this configuration is limited to around 100 grams.

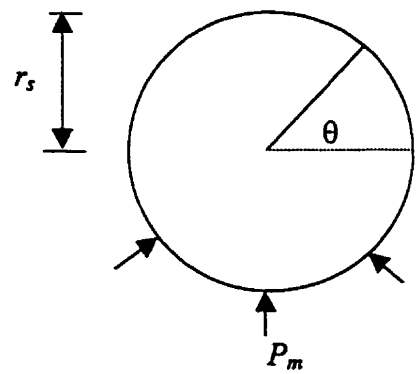

Figure 1-3, Pressure Distribution on a Molten Sphere

1.4 Levitation of a Metallic Torus

In this thesis, the levitation of a metallic torus was studied (Figure 1-4). The motivation for studying this system is to increase the amount of molten metal that can be levitated for metallurgical purposes. It was previously stated that the typical spherical levitation device cannot apply a magnetic pressure at the lowest point on the load. Therefore it depends on surface tension to prevent molten metal from leaking out. The toroidal geometry has an advantage over the spherical geometry. The torus does not have any material located on the axis of symmetry. It is therefore possible to design an induction coil, using a suitable arrangement of axisymmetric current-loops, such that no magnetic hole exists on the bottom surface of the load. Such a system would have no dependence on surface tension, and would be capable of levitating a greater mass of molten metal.

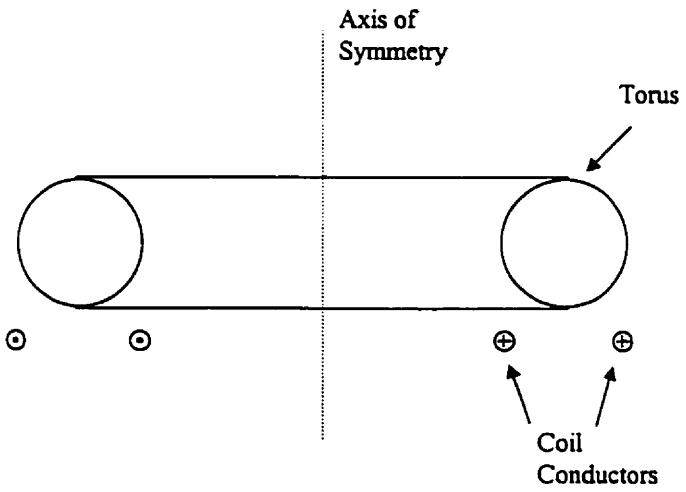

Figure 1-4, Toroidal Levitation System

1.5 Fundamental System Requirements

It was previously stated that levitation may occur when the bulk electromagnetic force balances the force of gravity acting on the load. When this is true, the load is in a state of equilibrium, as there is no net force acting upon it. However, this is not the only necessary condition for levitation. Sagardia [2] stated that there are three fundamental requirements that

must be satisfied for any levitation melting process to be successful. These requirements deal with bulk stability, surface stability and pressure distribution.

Bulk stability refers to the ability to keep the load, as a whole, levitating at a fixed equilibrium position. If the load is displaced from the equilibrium position, the system must restore the load back to the equilibrium position. It is necessary to have bulk stability to ensure that the molten load does not deform or break apart.

The surface stability refers to the system's ability to keep the surface of the molten load smooth and free from ripples. If a ripple forms on the surface, it is desired that the ripple should gradually disappear over time. If the ripple grows in amplitude, it could lead to a large distortion of the molten shape, possibly causing the load to break apart.

The magnetic pressure distribution must balance the hydrostatic pressure distribution on the surface to contain the molten metal. As previously mentioned, the typical spherical levitation device does not apply an appropriate pressure distribution on the surface of the sphere, and the system depends on surface tension to prevent molten metal from leaking out.

1.6 Thesis Objective

The primary objective of this thesis was to investigate the bulk stability of several toroidal levitation designs using both experiments and theoretical analysis. The experimental work was restricted to levitation of a solid load. This restriction simplifies the problem of levitation, as the requirements of pressure distribution and surface stability can be overlooked. Achieving bulk-stable levitation of a solid torus was considered to be the first step in developing a successful toroidal levitation melting system. Additional analytical work was done to determine magnetic pressure distributions and predict the cross-sectional flow pattern that would develop in the molten torus.

CHAPTER 2
LITERATURE REVIEW

There have been numerous papers published on the subject of spherical levitation, as this is the most common levitation system. Fewer references exist on the subject of levitation of a torus. However, much of the information on spherical levitation can be helpful in the study of toroidal levitation, so these references have been included in the literature review.

2.1 Levitation of Spherical Loads

The technique of electromagnetic levitation was first investigated in detail by Okress et al. [3]. The electromagnetic levitation melting of spherical loads was studied. They developed equations for the lifting force acting on a solid sphere in the presence of two coaxial current-loops. The current distribution in the sphere was modeled as an equivalent current-loop. The equations were verified through experiments. Levitation experiments were also performed using an induction coil similar to that of Figure 1-1. A number of different materials were successfully levitated in the solid state, including Copper, Aluminum, and Molybdenum. In one of several experiments, stable levitation of 21.5 g of molten Aluminum was achieved.

Peifer [4] discussed the state-of-the-art of levitation melting as of 1965. He stated the advantages and disadvantages of the technique. He summarized the work done regarding levitation forces, stability, induction coil design, temperature control and other aspects of levitation melting. He also gave a list of elements that have been successfully melted using the technique.

Gagnoud et al. [5] modeled the coupled aspects of the magnetic field and the free shape of the levitating molten load. The surface of the load was discretized into a number of coaxial rings. The currents in the rings were determined by solving for the magnetic vector potential. An iterative, variational method was used to determine the shape of the molten load.

Some studies have looked at the thermal and fluid dynamical aspects of levitation melting. El-Kaddah et al. [6] studied the levitation of a molten metal droplet. The coupled-circuits method was used to calculate the eddy-current distribution in the droplet, as well as

the bulk levitation force and power absorbed. The turbulent Navier-Stokes equations were solved numerically to determine the fluid flow field and temperature distribution in the droplet. Mestel [7] also solved for the fluid flow field inside a molten levitating sphere. A perturbation analysis was done in order to determine the shape of the molten load.

Several papers have discussed the issue of surface stability in levitating molten metal. Harris et al. [8] performed levitation experiments on molten Sodium immersed in an inert and transparent oil. The purpose was to identify mechanisms that may limit the amount of liquid metal that can be stably levitated. A wide range of excitation frequencies (between 100 Hz and 100 kHz) were used. Ripples were observed on the surface of the load during a majority of the experiments. It was stated that the ripples did not grow to a state of instability, possibly because the inert oil provided some damping against such behavior. It was observed that as the excitation frequency was increased, the wavelength and frequency of the surface ripples increased, while the amplitude decreased.

Sagardia [2] stated the three requirements that must be satisfied for a levitation system to be successful. The subject of surface stability was studied. It was determined that a single induction coil was not sufficient for providing absolute surface stability. Sagardia also developed a levitation device capable of suspending large spherical loads. The levitation device consisted of three independent coils, each coil having an individual power supply and frequency. The levitation melting of spherical Aluminum loads between 0.5 and 1.5 kg was achieved.

Krishnan et al. [9] performed levitation experiments on small metallic droplets. It was observed that the molten droplets experienced axisymmetric oscillations and rotations during the levitation process. An attempt was made to explain this dynamic behavior. Such oscillations are not always undesirable. In fact, this behavior can be used to calculate the surface tension of molten metals. This is called the levitated droplet method. If the droplet has a mass m, and oscillates at a frequency of ω, the surface tension γ is given by the formula:

$$\gamma = \frac{3\pi m\omega^2}{8} \tag{2.1}$$

Numerous papers have discussed the levitated droplet method. In particular, Kasama[10] used the method to measure the surface tension of liquid Iron and Iron-Oxygen alloys.

Chung[11] used the method to study the effect of oxygen on the surface tension of liquid Chromium. Levitation melting has been used to measure other high-temperature thermophysical properties. Mills et al. [12] discussed the use of the levitating droplet technique for determining density and enthalpy of fusion of liquid metals and alloys.

There are several studies regarding bulk stability of levitation systems. Brisley et al. [13] developed expressions for the vertical force acting on a solid sphere in the presence of several axisymmetric current-loops. The analysis assumed that the induction coil was current-driven, meaning that the peak current flowing through the induction coil was fixed. Analytical expressions for the levitation force were derived in terms of Legendre Polynomials. A curve was plotted to illustrate the nature of the levitation force as a function of levitation height. The slope of the force curve was used to explain the bulk stability of the system.

Hatch [14] described the bulk stability of a levitation system in terms of a potential well. The force acting on a conducting sphere was derived as the negative gradient of a scalar electromagnetic potential function. He also stated that the AC magnetic levitation of a nonmagnetic body was similar to DC levitation of a non-magnetic superconducting body. In both cases, the levitating force relies on the bulk diamagnetism of the levitating body. The potential well description was applied to several levitation systems consisting of two-loop induction coils.

Holmes [15] developed a simplified method for determining levitation force and analyzing the bulk stability of levitation systems. The sphere was treated as an equivalent magnetic dipole moment. It was shown that magnetic materials (having $\mu >> \mu_o$) cannot be levitated stably. The bulk stability of single and multi-loop induction coils was analyzed with respect to vertical and horizontal displacements.

Essmann et al. [16] observed bulk-stability problems during the electromagnetic levitation of metal specimens. The initial goal was to decarburize and degas a Niobium sphere. The problems encountered were two-fold: 1) movements of the load's center of gravity, and 2) rotations of the load. The movements of the center of gravity were caused by modulations of the applied voltage. The stability was improved by modifying the power supply so that the modulations were reduced. A superimposed DC magnetic field was used to

reduce the load rotation. It was observed that the rotation speed of the load was reduced to approximately one revolution per second.

Zhevnyak et al. [17] analyzed the effects of the structural dimensions of the induction coil on the bulk stability of a levitating sphere. The study was limited to single-loop and two-loop coils. It was assumed that the dimensions of the load were much smaller than the characteristic dimensions of the induction coil. It was shown that a single-loop coil must levitate the load within a very small range of space to achieve bulk stability. The upper limit on levitation height was due to lack of horizontal bulk stability, while the lower limit was due to lack of vertical bulk stability. This explains why stable levitation with a single-loop coil is difficult, if not impossible to achieve in practice.

2.2 Levitation of Cylindrical Loads

The levitation of a conducting cylinder has some similarity with the toroidal levitation system. This system has been studied by Piggott et al. [18]. The apparatus consisted of a long conducting cylinder placed above two parallel conductors carrying equal and opposite currents. Analytical expressions were developed for the levitation force, torque and power dissipation in the cylinder. An Aluminum cylinder 18 cm long and 2 cm in diameter was stably levitated.

Sneyd et al. [1] analyzed a levitation system consisting of an infinite cylinder levitated by two parallel conductors carrying equal currents in the same direction. This cylinder was conceived to be a section of a torus, having a mean radius r_a much larger than the cross-sectional radius r_b. The equations for vertical and horizontal forces acting on the cylinder were developed using the method of image-currents. The force equations were used to determine the necessary conditions for vertical equilibrium, vertical bulk-stability and horizontal bulk-stability. The fluid flow field and the cross-sectional shape of the molten load were also determined.

2.3 Levitation of Toroidal Loads

Vutsens [19] proposed a levitation system to overcome the problems associated with the magnetic hole of the typical spherical levitation system. The induction coil for this system

consisted of a number of coaxial loops, plus a current-carrying rod placed on the axis of symmetry (Figure 2-1). Experiments were performed using a Sodium load immersed in transparent oil. Stable levitation of the molten load was achieved. The load assumed the shape of a solid of rotation, topologically similar to a torus.

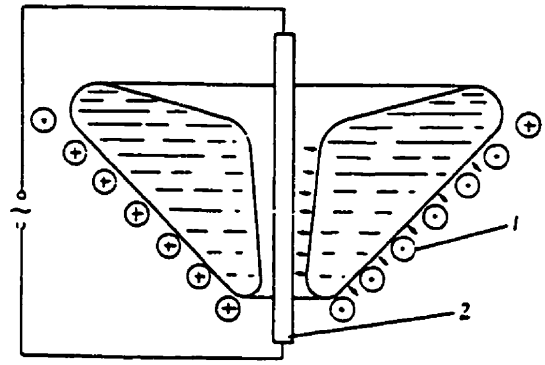

Figure 2-1, Induction coil used by Vutsens [19]

In a subsequent paper [20], Vutsens analyzed the electromagnetic field problem of a conducting torus freely levitating above a current-carrying loop. The analysis assumed that the excitation frequency is so high that the load behaves like a perfect conductor. Closed-form solutions were derived for induced current and pressure distribution on the surface of the torus, as well as the bulk levitation force.

Bendzsak [21] described an algorithm for designing an induction coil for a levitation system. The goal was to determine a coil design that would produce an electromagnetic pressure distribution to balance the hydrostatic pressure distribution on the surface of a levitating load. The algorithm was applied to the design of a toroidal levitation system. The pressure distribution on the surface of a torus was calculated using the analytical expressions from [20]. For the final coil design, the pressure distribution was shown to match the hydrostatic pressure distribution very closely.

CHAPTER 3
THEORETICAL ASPECTS

3.1 Introduction

In this chapter, the theoretical aspects of the levitation of a solid torus are discussed. There are essentially two systems to be examined: the electromagnetic system and the mechanical system. The electromagnetic system can be described in part using an equivalent electric circuit. However, a more accurate description of the electromagnetic system requires the evaluation of the induced current density in the load and the magnetic flux density vector. The interaction between induced current and magnetic field gives rise to electromagnetic forces acting on the load. The mechanical system describes how the load will respond to the electromagnetic and gravitational forces acting upon it.

3.2 Theory of Induction

At the heart of electromagnetic levitation is the principle of induction. When an open-circuited, conducting loop is in the presence of a time-varying magnetic field, a voltage V will be generated between the two terminals (Figure 3-1). According to Faraday's Law, this induced voltage is proportional to the rate of change of the total magnetic flux ψ_m passing through the loop.

$$V = -\frac{d\psi_m}{dt} \tag{3.1}$$

The total magnetic flux, measured in Webers, is obtained by integrating the magnetic flux density vector **B** over the entire area S inside the loop.

$$\psi_m = \iint_S \mathbf{B} \cdot \hat{\mathbf{n}} dS \tag{3.2}$$

$\hat{\mathbf{n}}$ is the unit vector normal to the elemental surface area dS. If the loop is short circuited, the induced voltage will generate a current. The current will tend to flow in a direction that creates opposition to the changing magnetic field that produced it. This effect is known as Lenz's Law.

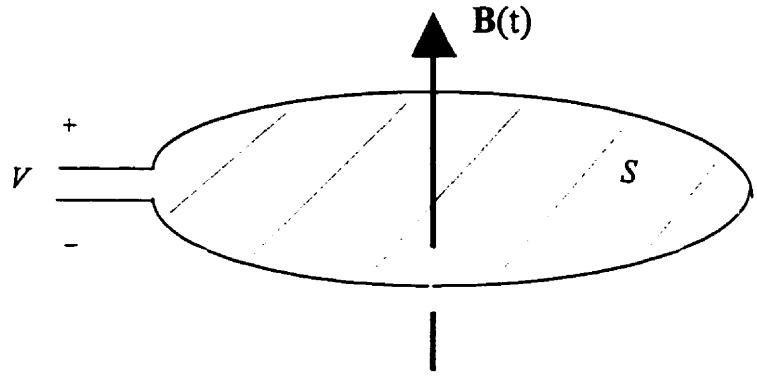

Figure 3-1, Faraday's Law

The principle of induction is essential in AC electrical systems. The self inductance and mutual inductance are two quantities that are generally used to model such systems. Both quantities are measured in Henrys. Consider a single filament loop, carrying a constant current I as shown in Figure 3-2. The magnetic field lines produced by the current form closed loops that pass through, or 'link' the current-loop. The number of flux linkages is equal to the total magnetic flux ψ_m passing through the loop. The self inductance L is defined as the ratio of total magnetic flux linkage to the current in the loop.

$$L = \frac{\psi_m}{I} \tag{3.3}$$

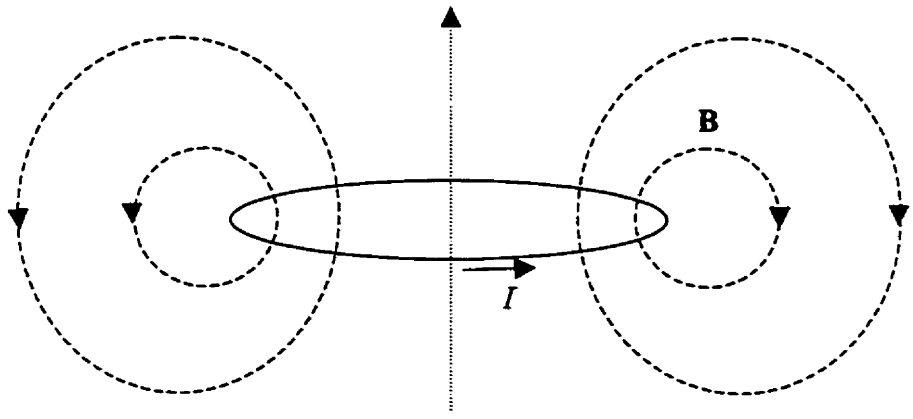

Figure 3-2, Self inductance of a single loop

The closed-form expression for the self inductance of a circular filament loop is given in the Appendix. When a time-varying current flows through the loop, the induced voltage between the two terminals of the loop is:

$$V = L\frac{dI}{dt} \tag{3.4}$$

In AC problems, both V and I are sinusoidal functions of time. It is therefore convenient to use the phasors **V** and **I**. In phasor notation, Equation 3.4 can be rewritten as:

$$\mathbf{V} = j\omega L\mathbf{I} \tag{3.5}$$

The mutual inductance is a measure of the extent of flux-linkage between two adjacent loops. Consider the two coplanar loops shown in Figure 3-3.

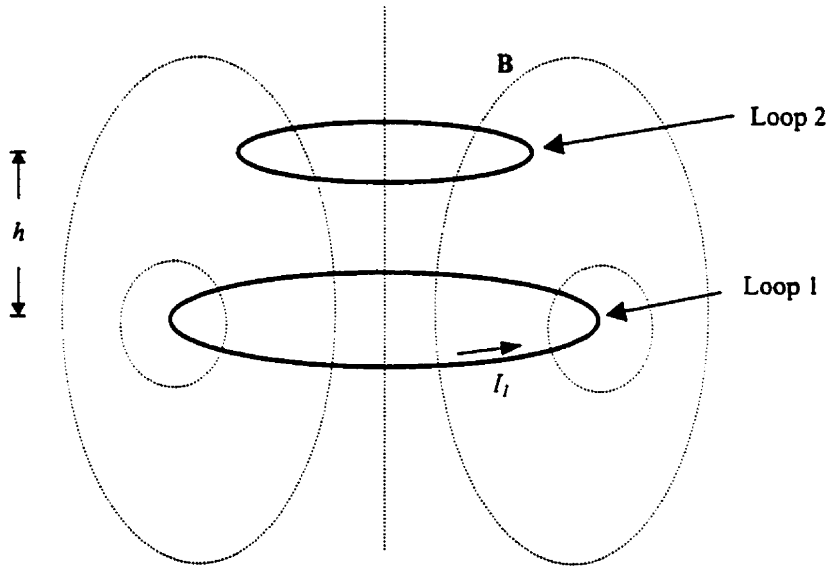

Figure 3-3, Mutual inductance between two loops

If Loop 1 carries a current I_1, a portion of the magnetic flux generated by the current will link Loop 2. This is sometimes called a magnetic coupling, or a coupled circuit. The mutual inductance between loops 1 and 2 is defined as the ratio of magnetic flux linkage through Loop 2 to the current flowing in Loop 1.

$$M_{12} = \frac{\Psi_{12}}{I_1} \tag{3.6}$$

Expressions for the mutual inductance are listed in the Appendix. The voltage $\mathbf{V}_2$ induced in Loop 2 due to the current $\mathbf{I}_1$ flowing in Loop 1 is:

$$\mathbf{V}_2 = j\omega M_{12}\mathbf{I}_1 \tag{3.7}$$

The mutual inductance is strongly dependent on the separation height and orientation of the two loops. For example, the mutual inductance between two coaxial loops is plotted as a function of separation height h in Figure 3-4. Both loops are assumed to have a radius of 10 cm.

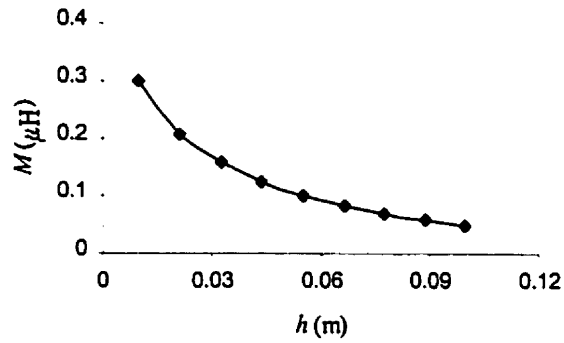

Figure 3-4, Plot of mutual inductance vs. height
for two coaxial loops

As the separation height increases, the amount of flux linking the two loops decreases. Since the mutual inductance is a measure of the amount of flux linkage, it also decreases with increasing separation height.

3.3 The Electric Circuit

A simplified electric circuit diagram of the levitation system is shown in Figure 3-5. The circuit consists of the power supply, the induction coil, and the torus. The resistances in the circuit are assumed to be negligible for the sake of simplicity. The power supply is assumed to apply an alternating voltage signal at a constant frequency. This is called a voltage-driven system, because the peak voltage can be kept at a constant value. The induction coil can be approximated using a number of axisymmetric current-loops. The self inductance of the coil L_C can be determined using the formula:

$$L_C = \sum_{i=1}^{m}\sum_{k=1}^{m} M_{ik} \tag{3.8}$$

where m is the total number of loops in the induction coil. When $i=k$, M_{ii} is the self-inductance L_i of the ith loop.

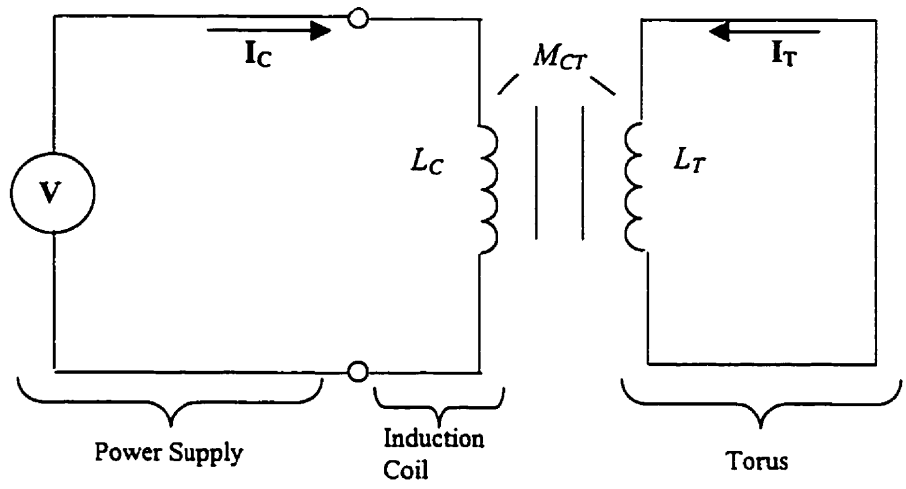

Figure 3-5, Electric Circuit

The torus is located directly above the induction coil. In the simplest analytical terms, the torus is a conducting loop. As such, it can be modeled as a closed circuit carrying a single current $\mathbf{I_T}$. The torus has a self inductance L_T. The magnetic field produced by the coil links the torus, creating a magnetic coupling. The extent of this coupling can be represented by a mutual inductance M_{CT}. Equations for the currents $\mathbf{I_T}$ and $\mathbf{I_C}$ can be written using Kirchoff's Voltage Law:

$$\mathbf{I_T} = -\frac{M_{CT}}{L_T}\mathbf{I_C} \tag{3.9}$$

$$\mathbf{I_C} = \frac{\mathbf{V}}{j\omega\left[L_C - \dfrac{M_{CT}^2}{L_T}\right]} = \frac{\mathbf{V}}{j\omega L_{eq}} \tag{3.10}$$

where L_{eq} is the equivalent self inductance of the circuit as perceived by the power supply. As Figure 3-4 illustrates, the mutual inductance between two coupled loops is affected by

changes in the position of one loop with respect to the other. It is reasonable to assume that M_{CT} will depend on the position of the levitating load with respect to the coil. Since the currents flowing in the load and the coil are dependent on the mutual inductance, they too are affected by changes in position of the load.

3.4 Induced Current Distribution

In the electric circuit model, a single variable $\mathbf{I_T}$ represents the induced current flowing in the load. In order to perform a more accurate analysis, it is necessary to consider the distribution of the induced currents in the load. Several methods may be used to solve this magnetic problem. An analytical method was developed by Vutsens [20]. His analysis assumed that the excitation frequency was sufficiently high so that the torus could be considered as a perfect conductor. In this case, the magnetic field does not penetrate beneath the surface of the torus. On the surface, only the tangential component of the magnetic field exists. The problem was solved in terms of the magnetic vector potential **A**. This is related to the magnetic flux density vector through the equation:

$$\nabla \times \mathbf{A} = \mathbf{B} \tag{3.11}$$

Because the problem is axisymmetric, only the ϕ component of **A** (A_ϕ) exists. The solution to the magnetic problem reduces to the solution of the Laplace equation for A_ϕ:

$$\nabla^2 A_\phi = 0 \tag{3.12}$$

with the boundary condition $A_\phi = 0$ on the surface of the torus. The method allows one to calculate both the surface current density and the magnetic flux density on the surface of the load. However, the resulting expressions are mathematically rigorous, and it was decided not to use them for this thesis.

As an alternative to this approach, the coupled-circuits method was used to determine the induced current distribution in the load. The essence of this method is that the load and the coil can be represented by a number of conducting loop elements. The coupled-circuits representation of the toroidal levitation system is shown in Figure 3-6. The induction coil is modeled using m loop elements, and the surface of the load is modeled using n loop elements. The entire system consists of p elements, where $p = m+n$. The index numbers 1 through m represent the coil elements, while the numbers m+1 through p represent the load elements.

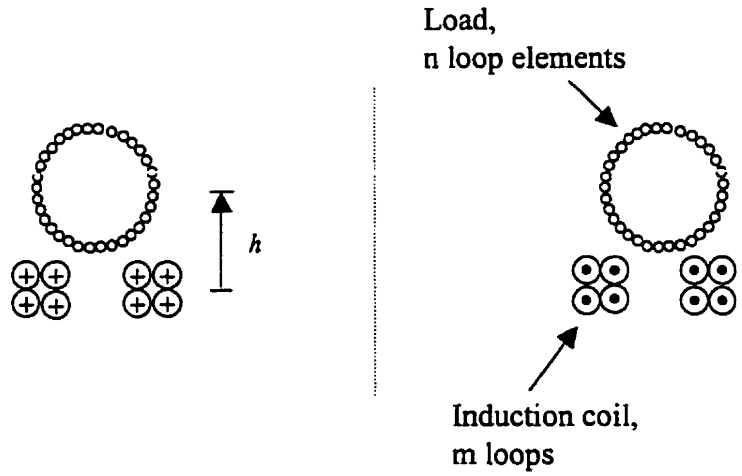

Figure 3-6, Coupled-circuits model

The load elements are located on the surface of the torus, since at high frequencies, the induced currents flow in a region very close to the surface. The thickness of this region is approximately equal to the electromagnetic penetration depth δ, where

$$\delta = \sqrt{\frac{2}{\omega\mu\sigma}} \tag{3.13}$$

For the experiments in this thesis, the penetration depth was approximately 0.06 cm. This is based on an excitation frequency of 15 kHz, a magnetic permeability of $\mu_o = 4\pi \times 10^{-7}$ H/m, and the conductivity of Aluminum at room temperature $\sigma = 3.8 \times 10^7 (\Omega m)^{-1}$. The cross-sectional diameter of the load elements was set to δ in order to model the current-carrying region accurately.

An equivalent circuit can be drawn for each of the p elements. Each element has a resistance R_i, and a self-inductance L_i. Each element is mutually coupled to all other elements in the model, with the mutual inductance between elements i and k denoted by M_{ik}. There may be a voltage V_i applied to the element, and a current I_i flowing through the element. Employing Kirchoff's Voltage Law, the equation for the ith element is:

$$V_i = R_i I_i + j\omega \sum_{k=1}^{p} M_{ik} I_k \tag{3.14}$$

By definition, when $i = k$, M_{ii} represents the self-inductance L_i. A set of p linear equations of this form can be written. In matrix form, the set of equations becomes:

$$\{V\} = [[R] + j\omega[M]]\{I\} \tag{3.15}$$

$\{V\}$ is the column vector representing the applied voltage to each element. $[R]$ is the resistance matrix. $[M]$ is the inductance matrix, containing the self and mutual inductances. $\{I\}$ is the column vector representing the current flowing through each element. In this thesis, it was assumed that all resistance terms in the model are zero. In reality, the resistance terms are not zero, since a significant amount of heat is generated due to power dissipation in the load. However, the zero-resistance assumption simplifies Equation 3.15 to the form:

$$\{V\} = j\omega[M]\{I\} \tag{3.16}$$

The problem of determining the current distribution in the load reduces to finding the solution for $\{I\}$ in Equation 3.16. This can be done using any computer program capable of matrix-manipulation. Additional details regarding the use of the coupled-circuits method are given in the Appendix.

A computer program was written to implement the coupled-circuits method for the toroidal levitation system. The program was tested against Vutsens' analysis by solving a common example problem, illustrated in Figure 3-7. The problem consists of a torus freely levitating above a current-carrying loop.

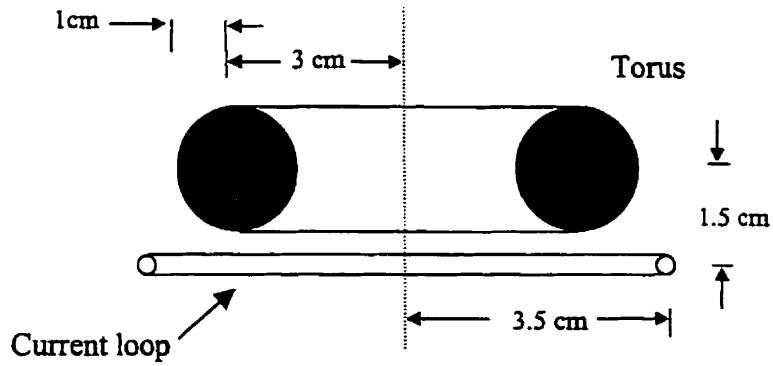

Figure 3-7, Example Problem

The loop carries a peak current of 1000 A. The torus is assumed to be levitating 1.5 cm above the loop. In Vutsen's model, the current flows on the surface of the torus only, and the current distribution is described by the r.m.s. surface current density **j** (measured in Amperes per meter).

For the coupled-circuits method, the individual currents in the load elements were converted into values for surface current density by dividing the current by the cross-sectional diameter of the element.

$$\mathbf{j}_i = \frac{I_i}{\delta}, \text{ for } i = m+1..p \tag{3.17}$$

Dividing this result by $\sqrt{2}$ gives the r.m.s. value. The surface current distributions obtained using Vutsens' method and the coupled-circuits method are shown in Figure 3-8. It is clear that the coupled-circuits method and the analytical method used by Vutsens produce very similar results.

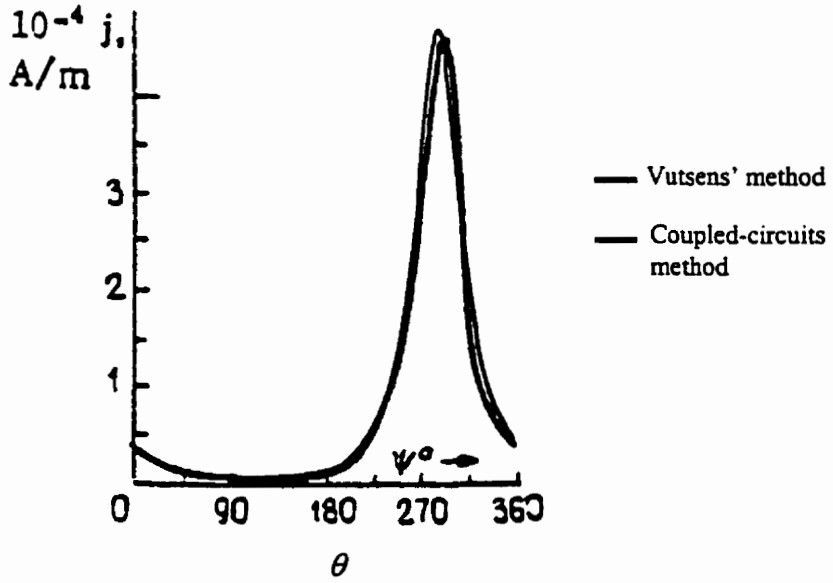

Figure 3-8, Plot of surface current density,
as determined by Vutsens' method and the coupled circuits method

3.5 Magnetic Flux Density

The magnetic flux density can be calculated at any point once the currents in all elements have been determined. At any point (r,z) in the axisymmetric cylindrical co-ordinate system, **B** has two components; an axial component B_z and a radial component B_r. Expressions for B_z and B_r due to a single current-carrying loop are given in the Appendix. The total **B** field produced by all elements in the model can be found using the principle of superposition. A convenient way of visualizing the magnetic field is to plot the streamlines of **B**. This is useful for identifying magnetic holes on the surface of the load. Regions where the streamlines are not tangential to the surface indicate places where the tangential magnetic field, and therefore, the magnetic pressure are zero.

In the axisymmetric-cylindrical coordinate system, the magnetic field streamlines are defined by the expression:

$$r \cdot A_\phi = const. \tag{3.18}$$

The expression for A_ϕ due to a single loop is also listed in the Appendix. The total value of A_ϕ at any point can be determined using superposition. Thus, a streamline plot can be generated by plotting the contour lines of the function $f = (rA_\phi)$ in the r-z plane.

3.6 Electromagnetic Force

When the current distribution and magnetic field are determined, the next step is to solve for the bulk electromagnetic forces acting on the load. Consider one of the n elements representing the surface of the load. The Lorentz force equation can be used to find the forces acting on the element, carrying a current **I** in the presence of an applied magnetic field $\mathbf{B}_a$. It should be remembered that $\mathbf{B}_a$ is the magnetic field produced by the currents in the coil loops only. The time-averaged force acting on an infinitesimal length dl of the element is:

$$d\mathbf{F}_i = \tfrac{1}{2}\mathrm{Re}(\mathbf{I} \times \mathbf{B}_a^*)dl \tag{3.19}$$

If the load is coaxial with the coil, then the system is axisymmetric. The current vector **I** has a single component I_ϕ. The magnetic field has a radial component B_{ra} and an axial component B_{za}. This results in two components of force:

$$dF_{ri} = \tfrac{1}{2}\mathrm{Re}(I_\phi B_{za}^*)dl \tag{3.20}$$

$$dF_{zi} = -\tfrac{1}{2}\mathrm{Re}(I_\phi B_{ra}{}^*)dl \tag{3.21}$$

The vertical force acting on a loop element of radius r_a is found by integrating Equation 3.21 completely around the loop:

$$F_{zi} = \oint_{loop} dF_{zi} = -\pi r_a I_\phi B_{ra} \tag{3.22}$$

The bulk lifting force acting on the load is found by summing the lifting forces acting on all n elements in the load.

$$F_z = \sum_{i=m+1}^{p} F_{zi} \tag{3.23}$$

When the load is not displaced from the center, the net radial force is zero due to symmetry. When the load is displaced horizontally by a distance d, the net radial force can be determined by integrating Equation 3.20 completely around the loop:

$$F_{ri} = \oint_{loop} dF_{ri}\hat{\mathbf{r}}_i \cdot \hat{\mathbf{d}} \tag{3.24}$$

$\hat{\mathbf{r}}_i$ is the unit vector pointing from the centre of the loop to the point of integration, and $\hat{\mathbf{d}}$ is the unit vector pointing in the direction of the horizontal displacement. The left-endpoint-estimate (from Salas et al.[22]) was used to numerically calculate this integral. The bulk radial force can be found by summing the radial forces acting on all n elements of the load.

$$F_r = \sum_{i=m+1}^{p} F_{ri} \tag{3.25}$$

In addition, the load may experience a torque about one or more axes. However, only the bulk vertical and radial forces were considered in this thesis.

3.7 Mechanical System

The mechanical system is the other part of the levitation system that must be examined. The motion of the load is governed by the gravitational and electromagnetic forces acting upon it. Two types of motion were examined in this thesis: vertical displacement, illustrated in Figure 3-9, and horizontal displacement in Figure 3-10.

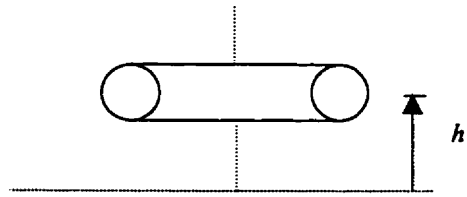

Figure 3-9, Vertical Displacement

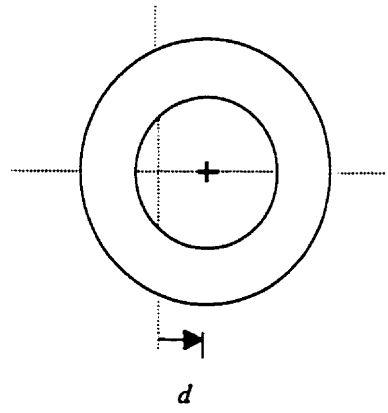

Figure 3-10, Horizontal Displacement

The load has two vertical forces acting upon it. The gravitational force is a constant downward force, given by the equation:

$$F_g = -mg\hat{z} \tag{3.26}$$

The electromagnetic lifting force F_z is generally positive, and varies depending on the levitation height h. When F_z is equal and opposite to the force of gravity, the load is in a state of equilibrium. The height at which this balance occurs is called the equilibrium height h_{eq}. The term 'bulk stability' is used to explain whether or not the load can be maintained at the equilibrium height. If the load is pushed slightly towards the coil, F_z must increase, tending to push the load back to equilibrium. On the other hand, if the load is raised slightly above the equilibrium height, F_z must decrease, allowing the load to fall back to equilibrium. In mathematical terms, this means that the slope of the vertical electromagnetic force curve must be negative in the region near the equilibrium position.

$$\left.\frac{\partial F_z}{\partial h}\right|_{eqm} < 0 \qquad (3.27)$$

If the slope of the force curve is negative, then the levitation system has vertical bulk stability. If the slope is zero or positive, then the levitation system does not have vertical bulk stability.

A similar statement can be made regarding horizontal displacement. In the horizontal direction, only the horizontal electromagnetic force F_r acts on the load. This force is generally a function of the radial displacement d from the axis of symmetry. When the load is in the center of the coil ($d = 0$), there is no net radial force due to symmetry, and the load is in equilibrium. However when the load is displaced in the horizontal direction, F_r must become negative, tending to push the load back to the center. This can be stated in terms of the slope of the horizontal force curve.

$$\left.\frac{\partial F_r}{\partial d}\right|_{eqm} < 0 \qquad (3.28)$$

If the force curve has a negative slope in the region near the center, the levitation system has horizontal bulk stability. Otherwise, the system does not have horizontal bulk stability.

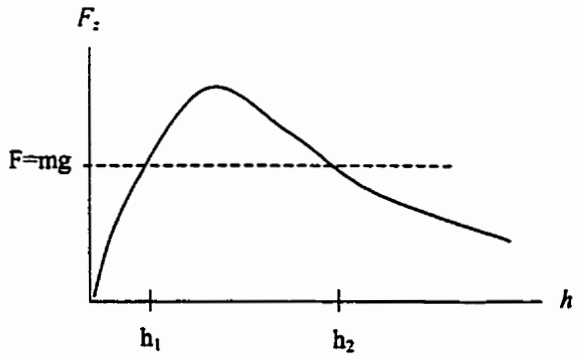

Figure 3-11, Example plot of vertical force curve

Information regarding the bulk stability of a levitation system can be obtained by plotting the force curves as a function of load displacement. Consider the vertical force curve shown in Figure 3-11. The dashed horizontal line indicates the weight of the load. The vertical force balances the weight at two different heights h_1 and h_2, but only one of these

represents a point of stable equilibrium. Since the slope of the force curve is positive in the region near h_1, this is a point where the levitation system is unstable. However, the slope is negative in the region near h_2, indicating that the system has vertical bulk stability at this point.

If the system has both vertical and horizontal bulk stability, and the load is initially displaced from the equilibrium position, the load will tend to oscillate about the equilibrium position. The motion of the load is governed by Newton's second law of motion $\mathbf{F} = m\mathbf{a}$, where $\mathbf{F}$ is the net force acting on the load, m is the mass of the load, and $\mathbf{a}$ is the acceleration of the load. An equation of this type can be written for both the vertical and horizontal directions.

$$F_z(h) - mg = m\ddot{h} \tag{3.29}$$

$$F_r(d) = m\ddot{d} \tag{3.30}$$

F_z and F_r are generally nonlinear functions. However, for small displacements about the equilibrium position, the vertical and horizontal forces may be approximated using a first-order Taylor expansion.

$$F_z(h) \cong mg + \alpha(h - h_{eq}) \tag{3.31}$$

$$F_r(d) \cong \beta d \tag{3.32}$$

where

$$\alpha = \left.\frac{\partial F_z}{\partial h}\right|_{h=h_{eq}} \tag{3.33}$$

$$\beta = \left.\frac{\partial F_r}{\partial d}\right|_{d=0} \tag{3.34}$$

The linear differential equations of motion become:

$$\ddot{h} = \frac{\alpha}{m}\left(h - h_{eq}\right) \tag{3.35}$$

$$\ddot{d} = \frac{\beta}{m} d \tag{3.36}$$

It can be shown (see Kittel et al. [23]) that the solutions for these differential equations are of the form:

$$h = h_{eq} + A_z \cos(\omega_z t) \tag{3.37}$$

$$d = A_r \cos(\omega_r t) \tag{3.38}$$

where

$$\omega_z = \sqrt{\frac{-\alpha}{m}} \tag{3.39}$$

$$\omega_r = \sqrt{\frac{-\beta}{m}} \tag{3.40}$$

The constants A_z and A_r are the amplitudes of oscillation in the vertical and horizontal directions respectively. These are determined by the initial displacements h_o and d_o from the equilibrium position.

The linearization of the force curves is only valid for small displacements about the equilibrium position. If large displacements occur, the higher order terms of the force curves must be considered. In this case, the differential equations of motion may be solved using the Runge-Kutta method or other numerical methods.

In all analyses, the induction coil was assumed to be energized by a 15 kHz signal, with a peak voltage of 200 V. The exact voltage was not recorded for each experiment. However, in much of the analytical work, the emphasis was placed on studying bulk stability. This is largely dependent on the slope or shape of the force curves, rather than the actual magnitude of the forces. It can be shown that the force acting on the levitating load is proportional to the square of the applied voltage. Therefore, despite the fact that the magnitudes of the forces are not necessarily identical to those from the experiment, the basic features of the force curves are accurate.

CHAPTER 4
EXPERIMENTAL ASPECTS

4.1 Apparatus

A schematic diagram of the experimental apparatus is shown in Figure 4-1. The apparatus consisted of four main components: the power supply, the auto-transformer, the induction coil and the load.

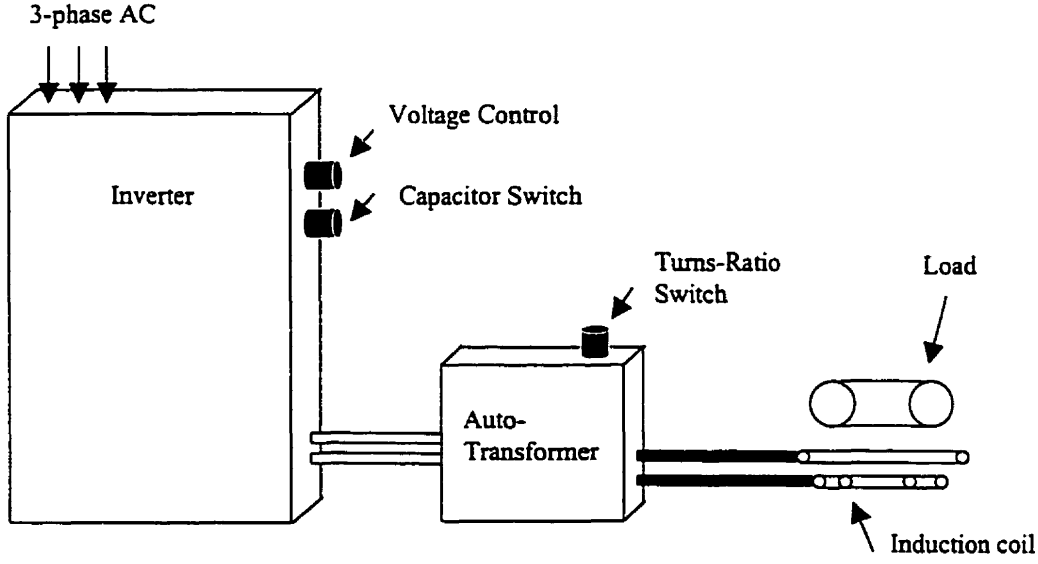

Figure 4-1, Diagram of Apparatus

A solid-state inverter was used as the power supply. The inverter performs two major functions: rectification and inversion. First, the inverter converts the three-phase AC voltage into a DC voltage, V_{DC}. Second, the inverter converts the DC voltage into a sinusoidal output voltage V, having an angular frequency ω. The voltage can be adjusted using the voltage control knob. The inverter used was a Radyne Type 20TQ50. It had a maximum output voltage of 1000 V r.m.s., and a maximum frequency of 50 kHz.

The autotransformer is a device that reduces the output voltage in exchange for an increased output current to the induction coil. A circuit diagram of the autotransformer is shown in Figure 4-2. The autotransformer has a primary winding with N_1 turns, and a

secondary winding with N_2 turns. The turns-ratio n (N_1/N_2) can be manually adjusted using the turns-ratio switch.

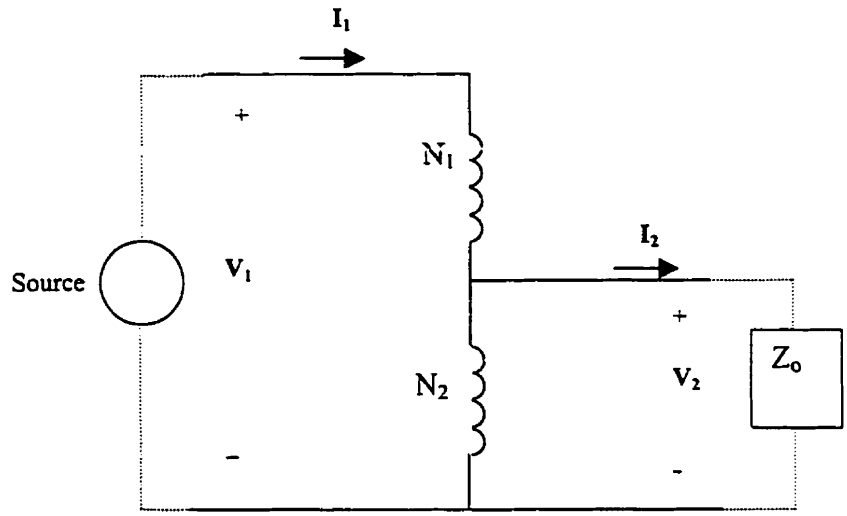

Figure 4-2, Circuit Diagram of Autotransformer

For an ideal autotransformer (from Irwin [24]), the relations between input and output voltage and current are:

$$\mathbf{V}_2 = \frac{1}{(1+n)}\mathbf{V}_1 \tag{4.1}$$

$$\mathbf{I}_2 = (1+n)\mathbf{I}_1 \tag{4.2}$$

If a load Z_o is connected to the output of the autotransformer, the equivalent impedance as seen by the power supply is:

$$Z_{eq} = (1+n)^2 Z_o \tag{4.3}$$

The output of the autotransformer is connected to the two input terminals of the induction coil. The induction coils used in experiments were made using ¼" or $^3/_{16}$" insulated Copper tubing. Water is pumped through the induction coil to prevent overheating. The load is placed directly on top of the induction coil, where it remains until the coil is energized, and the electromagnetic lifting force becomes strong enough to overcome the weight of the load.

4.2 Equivalent Electrical Circuit of Apparatus

The inverter applies a sinusoidal voltage to the output circuit, which consists of the autotransformer, the induction coil and the load. This can be approximated by an equivalent inductance L_{eq}. An adjustable capacitor, located within the inverter, is connected in parallel with the output circuit. This forms a resonating L-C circuit (Figure 4-3), having a resonant frequency:

$$\omega_{res} = \frac{1}{\sqrt{L_{eq}C}} \tag{4.4}$$

The capacitor can be adjusted from approximately 0.1 – 10 μF, and provides a means for tuning the circuit to the inverter. This enables maximum power transfer to the induction coil. The tuning process is done by trial and error. The value of capacitance can be manually adjusted using a switch on the inverter. The inductance of the output circuit can be manually adjusted by changing the value of n on the autotransformer. Different coil/load configurations have different impedances. Therefore, the tuning process was performed for each new experiment.

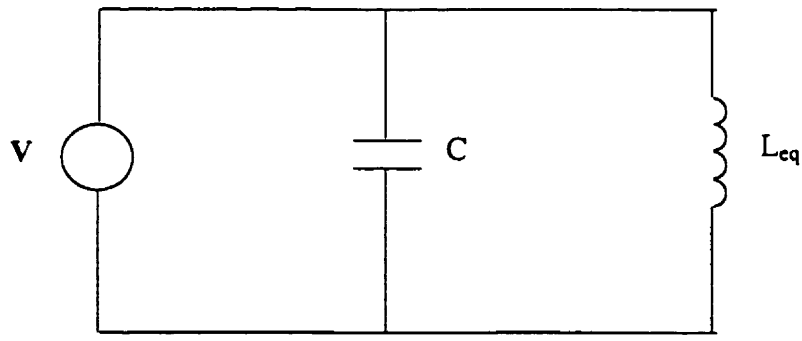

Figure 4-3, Resonant L-C Circuit

4.3 Loads

Three different loads were used in the levitation experiments: the filament loop, the torus, and the flat ring. The filament loop (Figure 4-4) was constructed by bending a piece of Copper tubing into a loop. The two ends of the loop were silver-soldered together. Silver solder was chosen over Lead-Tin solder because it has a higher melting temperature. This

load was built because of its low cost and easy construction. It had a weight of approximately 100 g. The cross-sectional radius was 0.47cm, and the mean radius was 10 cm.

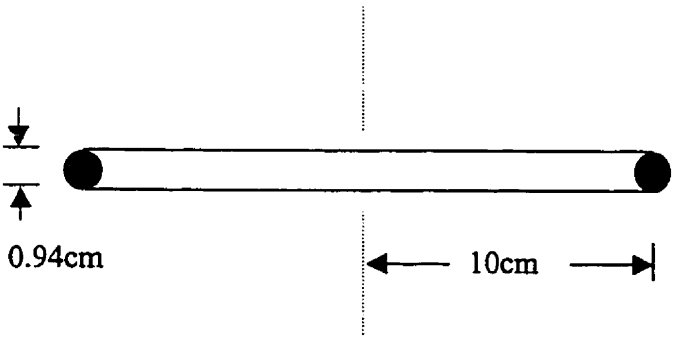

Figure 4-4, Filament Loop

The torus (Figure 4-5) was machined from a solid piece of Aluminum. It had a weight of approximately 470 g. The torus had a cross-sectional radius of 1.2 cm and a mean radius of 6.1 cm.

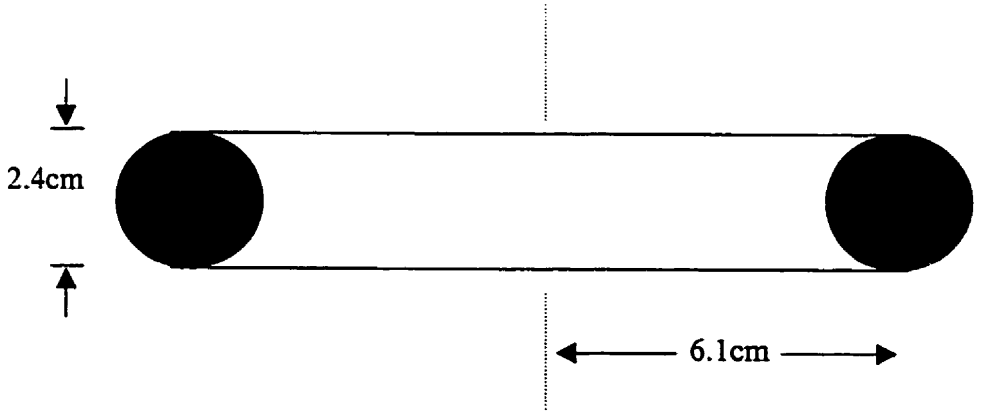

Figure 4-5, Torus

The flat ring (Figure 4-6) was constructed by cutting a ring out of a piece of Aluminum sheet, approximately 0.4 cm thick. The flat ring was used as an alternative to the filament load and the torus. It had a weight of approximately 83 g. The outer radius was 7.4 cm, and the inner radius was 4.8 cm.

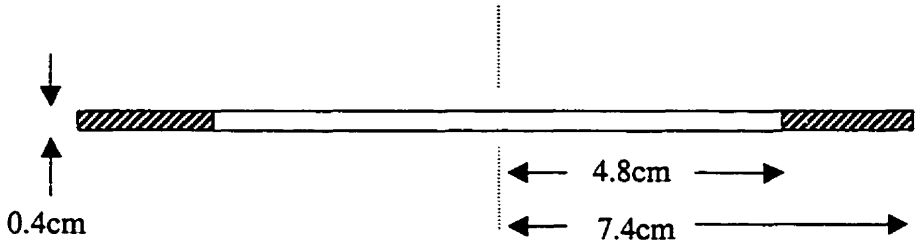

Figure 4-6, Flat Ring

4.4 Coil Design Considerations

The coil designs in this thesis consisted of a number of axisymmetric current-loops connected in series. In reality, the loops must be connected together by leads. The leads create end-effects which distort the magnetic field. An effort was made to reduce the end-effects in the coils. The lengths of the leads were kept as short as possible. If two parallel leads carried current in opposite directions, they were positioned very close to each other. In this way, the magnetic field produced by one lead cancels out the magnetic field produced by the adjacent lead, and the end effects are minimized. For example, the first coil design used in this thesis consisted of two concentric loops. Figure 4-7 shows how the leads were shaped in order to reduce the end-effects.

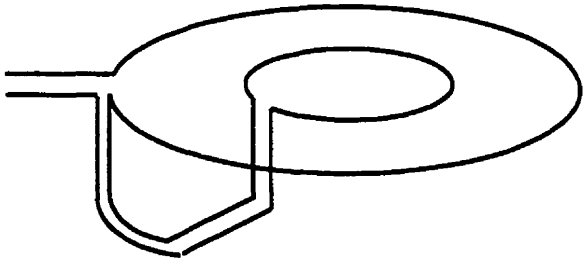

Figure 4-7, Coil designed to reduce the end-effects

CHAPTER 5
LEVITATION USING A TWO–LOOP COIL

5.1 Introduction

This chapter discusses the levitation of a toroidal load using a two-loop coil design. The two loops of the coil are concentric, and are wound such that the currents flow in the same direction. This coil design was studied because it is relatively simple to construct. Three two-loop schemes were studied, using both experiments and the analysis tools discussed in Chapter 3.

5.2 Scheme #1

The first scheme is shown in Figure 5-1. The filament loop was used as the load. The induction coil consisted of two loops with radii of 7.5 and 12.5 cm.

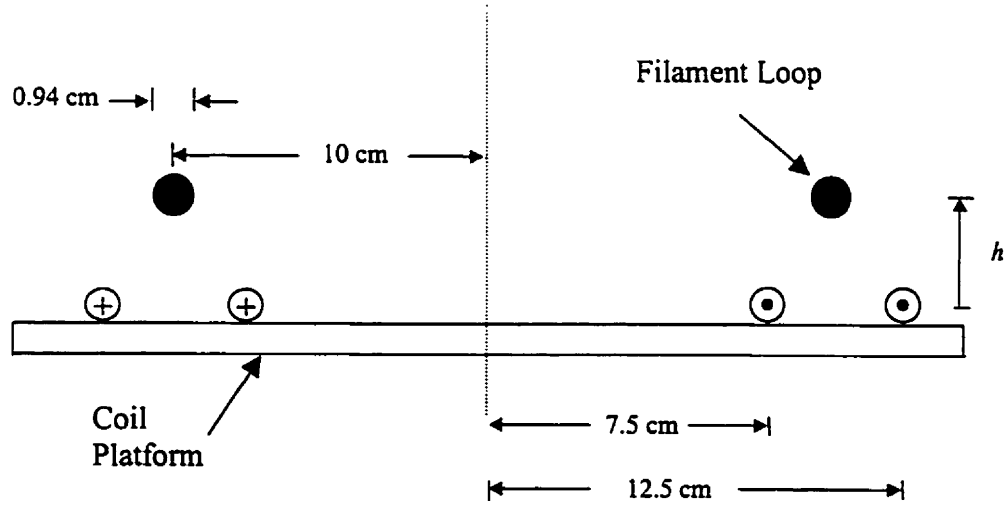

Figure 5-1, Two-Loop Scheme #1

Experiments

The experiments showed that this scheme was not capable of levitating the load stably. When the coil was energized, one side of the load would rise about 4 cm above the coil platform, while the opposite side rested on the platform (Figure 5-2). An attempt was made

to move the load with wooden sticks and push it into a stable position. This did not work, and it was clear that this scheme did not have bulk stability.

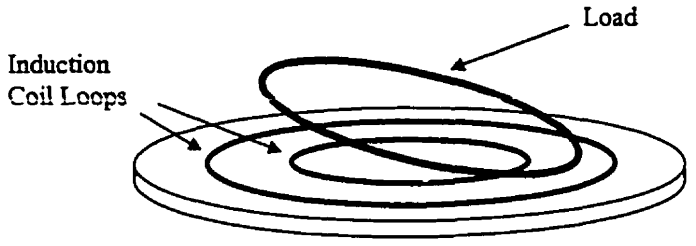

Figure 5-2, Experimental result for Two-Loop Scheme #1

Analysis

Figure 5-3 shows a plot of the magnetic field streamlines for Scheme #1. The load is levitating at a height of 20 mm. The large circle indicates the levitating load, and the quarter-circles in the two lower corners of the plot indicate the two loops of the induction coil. Figure 5-4 shows a plot of the vertical force curve. The curve has a local maximum at a levitation height of approximately 17 mm. Above this height, the slope is negative and vertical bulk stability is possible. Below 17 mm the slope is positive, and vertical bulk stability is impossible.

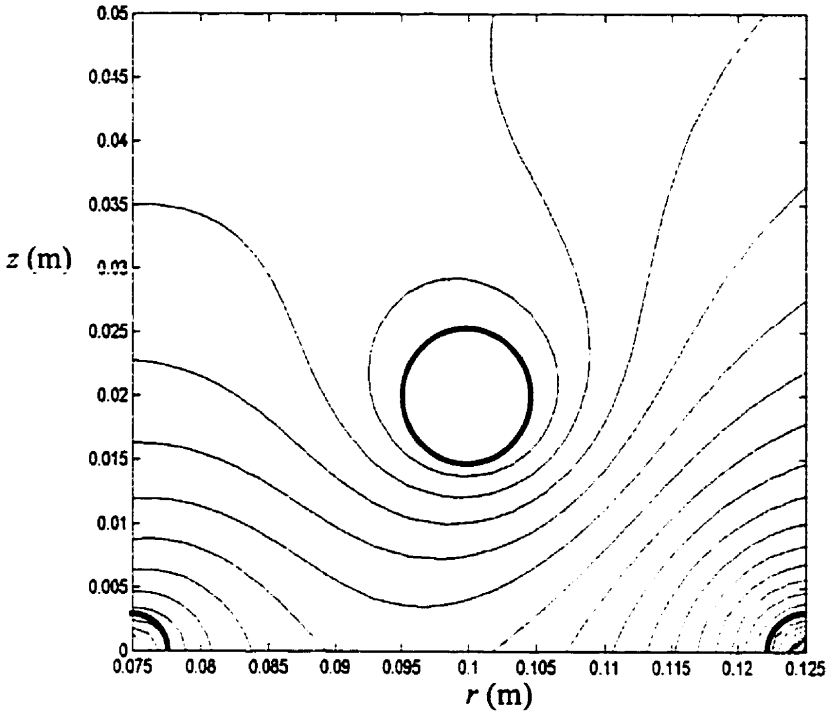

Figure 5-3, Streamline plot for Two-Loop Scheme #1

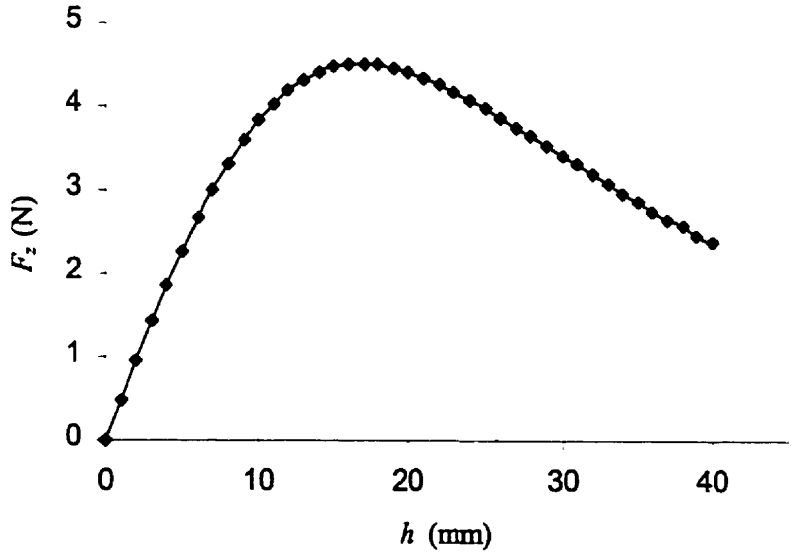

Figure 5-4, Vertical force curve for Two-Loop Scheme #1

Figure 5-5 shows a plot of the horizontal force curves for Scheme #1. The curves were plotted for levitation heights of 20, 25 and 30 mm. At 25 mm and 30 mm, the slope of the curve is always non-negative, indicating that horizontal bulk stability is impossible at these heights. At a height of 20 mm, the slope of the curve is negative for radial displacements less than 10mm, indicating that the system has horizontal bulk stability within this range.

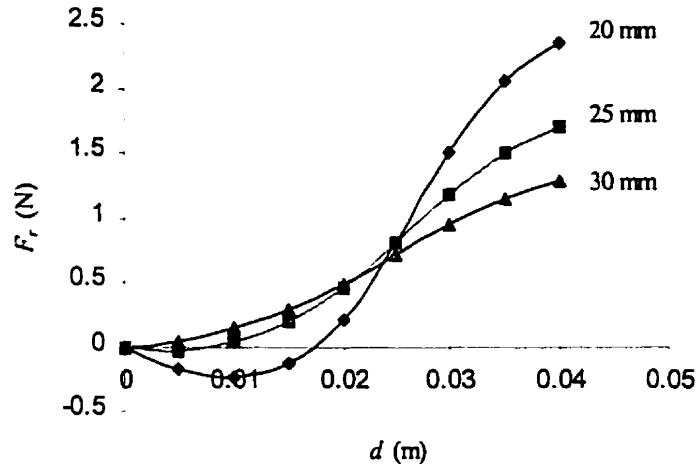

Figure 5-5, Horizontal force curves for Two-Loop Scheme #1

The force curves agree with the experimental results. At levitation heights below 17 mm, the system lacks vertical bulk stability. At levitation heights above 20 mm, the system lacks horizontal bulk stability. The load must remain levitating within this very small zone, between 17 and 20 mm, if the system is to have both vertical and horizontal bulk stability. This requirement is difficult to satisfy in practice, which is why bulk stable levitation was not achieved during the experiments.

5.3 Infinite Cylinder Analysis

Before investigating other two-loop levitation schemes, it is important to mention the work done by Sneyd et al. [1]. This paper discusses the levitation of an infinite cylinder using two parallel current-carrying loops. The cylinder was conceived to be part of a torus whose

mean radius r_a was much greater than the cross-sectional radius r_b. Figure 5-6 shows a diagram of this levitation system.

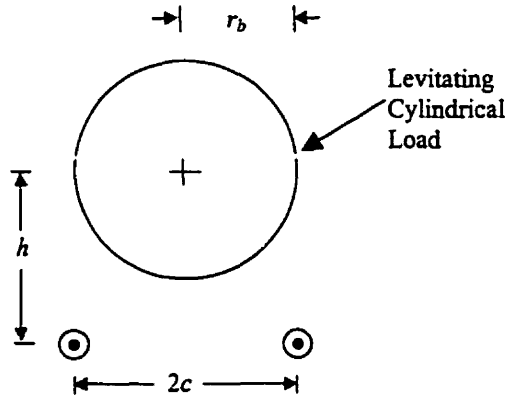

Figure 5-6, Levitation system considered by Sneyd et al. [1]

The relative size of the system is specified by the dimensionless variable $\kappa = r_b/c$, where c is one-half of the separation distance between the two conductors. The levitation height of the load is specified by the dimensionless variable $\eta = h/c$. The vertical electromagnetic force was expressed as:

$$F_z = \frac{\mu_o I}{2\pi c} G(\eta,\kappa) \tag{5.1}$$

where I is the peak current flowing in each conductor, and $G(\eta,\kappa)$ is a dimensionless function which depends only on the geometry of the levitation system. The peak current flowing through the conductors was assumed to be constant. Figure 5-7 shows a graph from [1], where $G(\eta,\kappa)$ is plotted as a function of η for different values of κ. The graph illustrates the nature of the vertical force and indicates regions where stable levitation can occur. The horizontal line (W) corresponds to the weight of the load, and can be located arbitrarily. The small vertical dash on each curve indicates the horizontal stability limit. The limiting value for η, below which the system has horizontal bulk stability, is given by the expression:

$$\eta_{max} = \sqrt{1+\kappa^2} \tag{5.2}$$

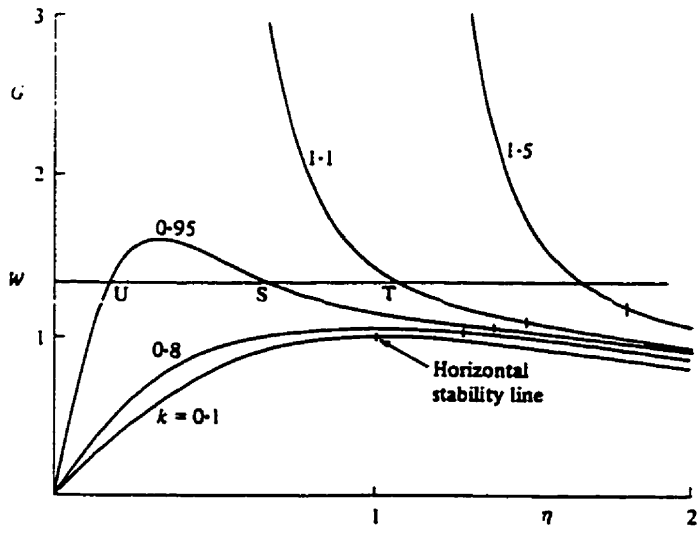

Figure 5-7, Graph from [1] showing curves of $G(\eta,\kappa)$ vs. η for different values of κ.

Consider the curve for $\kappa = 0.95$. The force balances the weight of the load at two points: U and S. However, at U the slope of the curve is positive, which indicates that the system does not have vertical bulk stability at this point. At S, the slope is negative and the system has vertical bulk stability at this point. The vertical dash indicates that the system has horizontal bulk stability up to approximately $\eta = 1.4$. Therefore, the curve predicts that stable levitation can be achieved with this design. Another successful design is realized for $\kappa = 1.1$. The equilibrium point occurs at T, and since the slope of the curve is negative at this point, the system has vertical bulk stability. The system also has horizontal bulk stability up to $\eta = 1.5$. Conversely, no region of stable levitation exists when $\kappa = 0.1$.

These results suggest that κ should be approximately unity in order to achieve stable levitation. In the study of Scheme #1, it was determined that the system could not stably levitate the load. The value of κ for that system was calculated to be 0.16. The results from the graph in Figure 5-7 also predict that such a system will be unstable. Therefore, it was decided to use the results from the infinite-cylinder analysis in the design of a new toroidal levitation scheme. The goal was to set $\kappa = 1$, and see if this could provide bulk stability.

5.4 Scheme #2

In the second scheme (Figure 5-8), a coil/load system was built such that the cross-sectional diameter of the load was equal to the spacing between the two loops of the induction coil. The torus was used as the load. The new coil was essentially a two-loop design, except each loop consisted of a bundle of four individual turns. A greater lifting force can be generated for a given current by increasing the number of turns in the coil. This was necessary since the torus was much heavier than the filament loop.

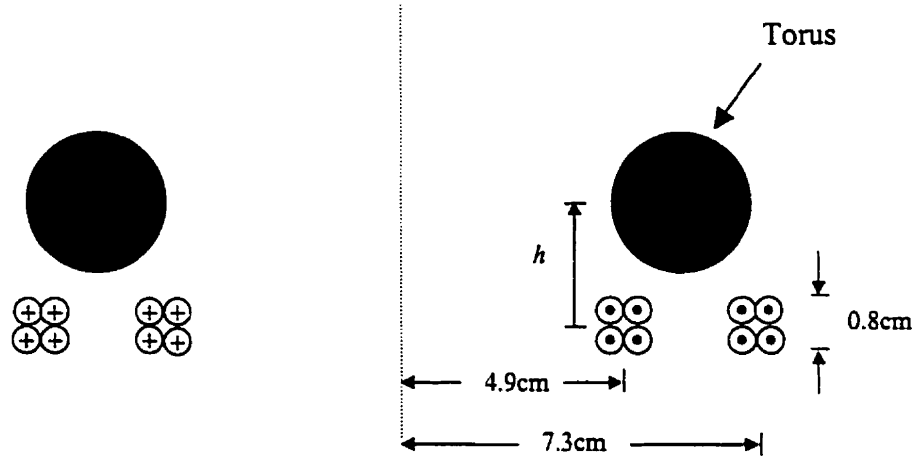

Figure 5-8, Two-Loop Scheme #2

Experiments

The experiments revealed that Scheme #2 was not capable of providing bulk stability. When the coil was energized, the torus would rise and move horizontally away from the axis of symmetry. This indicated that there was a lack of horizontal bulk stability.

Analysis

Figure 5-9 shows a plot of the magnetic field streamlines for Scheme #2. The load is at a levitation height of 20 mm. The plot illustrates the benefit of using the toroidal geometry, as there is no indication of a magnetic hole on the bottom surface of the load. Figure 5-10 shows a plot of the vertical force curve. The levitation height ranges from 14 mm to 30 mm.

The force curve is similar to that for Scheme #1, since there is a local maximum. This occurs at approximately 15 mm. The slope of the curve is negative for greater heights. Therefore, as long as the load is levitating above 15 mm, vertical bulk stability is possible.

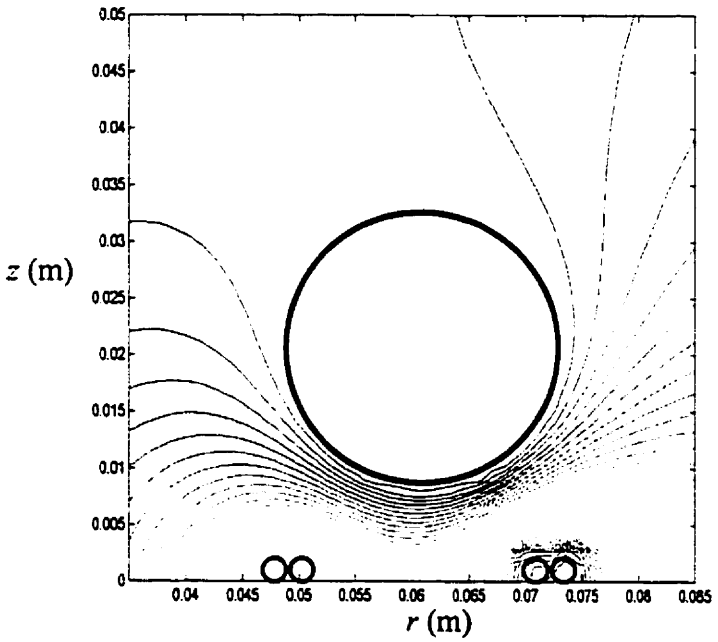

Figure 5-9, Streamline plot for Two-Loop Scheme #2

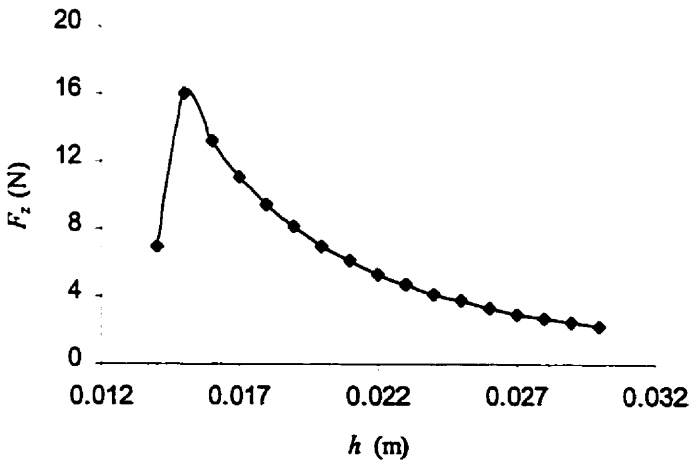

Figure 5-10, Vertical force curve for Two-Loop Scheme #2.

Figure 5-11 shows a plot of the horizontal force curves for Scheme #2. The curves are plotted for levitation heights of 15, 17, 20 and 25 mm, and for radial displacements up to 10 mm. The slope is always positive for all four curves, indicating that the system does not have horizontal bulk stability at these levitation heights. This explains why the load had a strong tendency to move in the horizontal direction during experiments. This coil cannot levitate the load because it does not provide horizontal bulk stability.

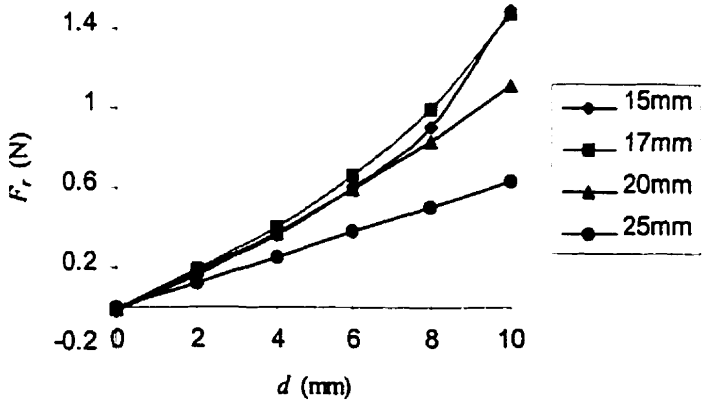

Figure 5-11, Horizontal force curves for Two-Loop Scheme #2

According to the infinite-cylinder analysis, there should be some region in which the system has both vertical and horizontal bulk stability. For $\kappa = 1$, the system should have horizontal bulk stability for levitation heights up to approximately 17 mm. However, the force plots at 15 mm and 17 mm from Figure 5-11 indicate that the system does not have horizontal bulk stability at these heights.

The discrepancy between the infinite cylinder analysis and the toroidal analysis was possibly related to the fact that the ratio r_a:r_b was only 5:1 in this scheme. It was believed that this ratio was not large enough to accurately describe the toroidal system using the infinite-cylinder analysis. It was decided to analyze the vertical and horizontal forces for the case when r_a:r_b = 20:1. The cross-sectional radius of the load was kept at 1.2 cm, while the mean radius of the load and the radii of the conductors were increased accordingly. Figure 5-12 shows a plot of the vertical force curve for the case r_a:r_b = 20:1. There is no local

maximum value and the slope is consistently negative. Vertical bulk stability can be achieved at all levitation heights.

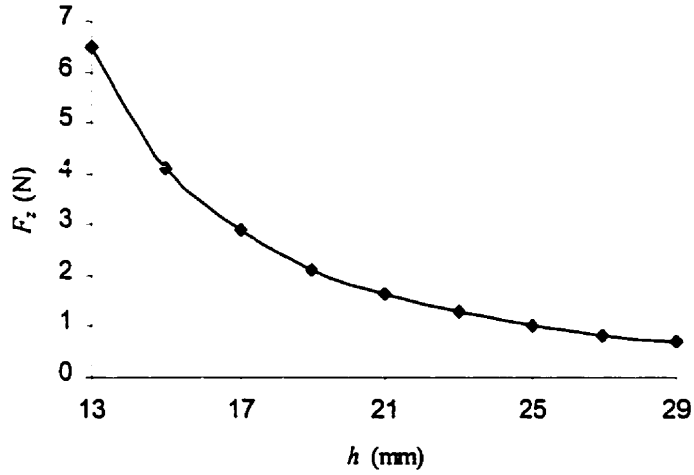

Figure 5-12, Plot of vertical force curve for Two-Loop Scheme #2, with r_a:r_b = 20:1

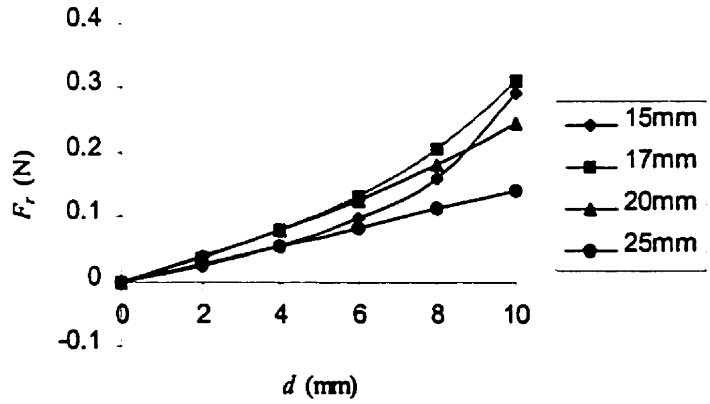

Figure 5-13, Horizontal force curves for Two-Loop Scheme #2, with r_a:r_b = 20:1

Figure 5-13 shows a plot of the horizontal force curves for levitation heights of 15, 17, 20 and 25 mm. The slopes are positive for all four curves, indicating that the system does not have horizontal bulk stability. Despite the fact that the radius ratio was increased to 20:1, the

results do not resemble those of the infinite cylinder analysis. At any rate, the experimental and analytical results show that this scheme is not capable of stably levitating a torus.

5.5 Scheme #3

Stable levitation was not obtained with the two previous schemes. It was decided to perform a simplified levitation experiment using a two-loop coil and a tethered load, as shown in Figure 5-14. A wooden pole was fixed on the axis of symmetry of the coil. The flat ring was used as the load. A washer was tied to the centre of the load using four pieces of string. In this way, the load was free to move in the vertical direction, but unable to move in the horizontal plane. By tethering the load to the centre, it was possible to study the system's vertical bulk stability alone, and neglect any consequences of the horizontal bulk stability.

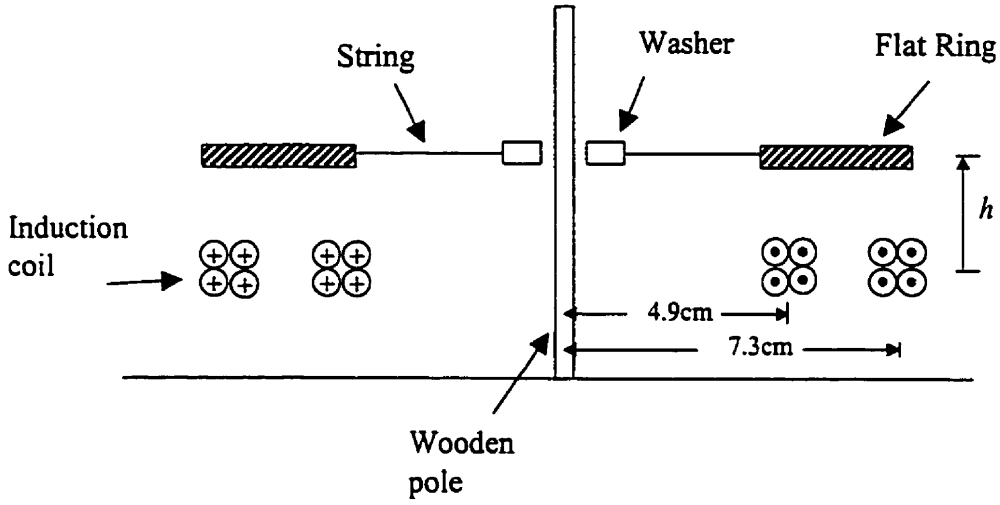

Figure 5-14, Two-Loop Scheme #3

Experiments

When the coil was energized, the load levitated at a height of approximately 2.5 cm. The load was level with the horizontal plane, and levitated in a virtually motionless state. However, when the tether strings were removed, the load moved horizontally away from the axis of symmetry, and stable levitation was not possible.

Analysis

Figure 5-15 shows a plot of the magnetic field streamlines for Scheme #3. Figure 5-16 shows a plot of the vertical force curve. The slope of the curve is always negative, so vertical bulk stability can be achieved at any height. Figure 5-17 shows a plot of the horizontal force curves. The curves are plotted for levitation heights of 10 mm, 20 mm and 30 mm. At all three levitation heights, the slope of the force curve is always positive, showing that the system does not have horizontal bulk stability at these heights.

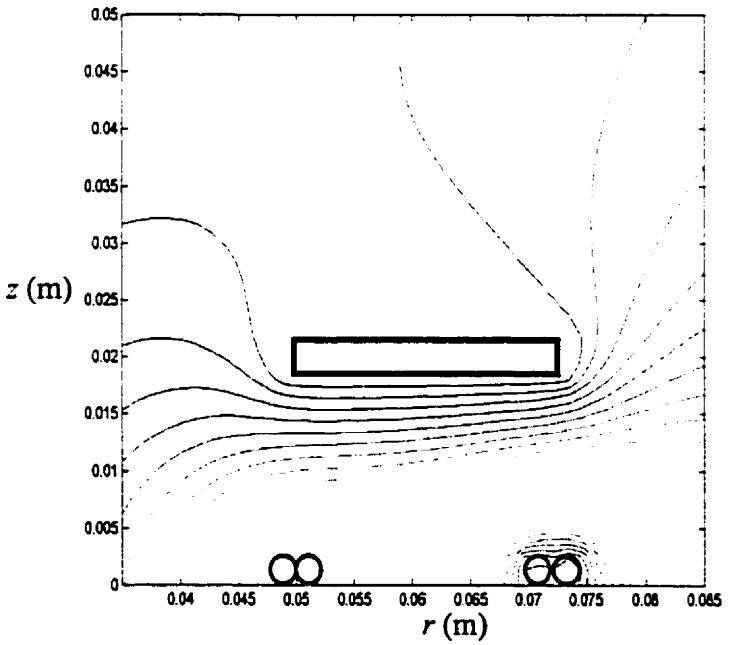

Figure 5-15, Streamline plot for Two-Loop Scheme #3

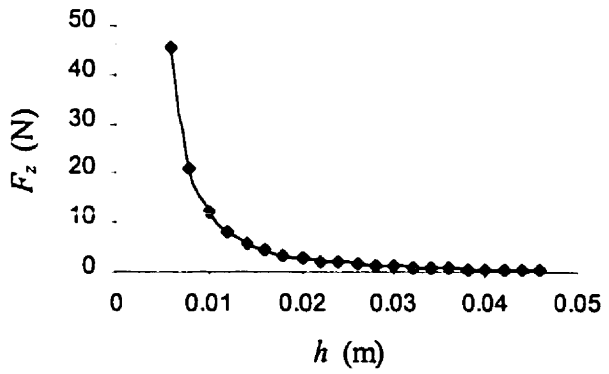

Figure 5-16, Vertical force curve for Two-Loop Scheme #3.

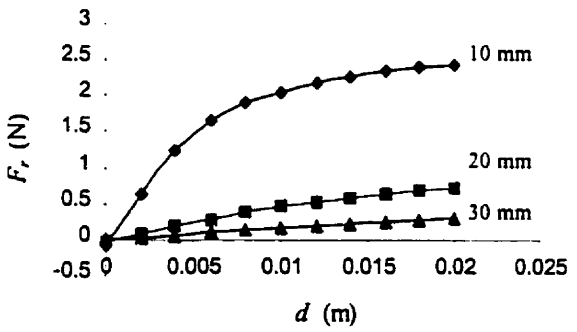

Figure 5-17, Horizontal force curves for Two-Loop Scheme #3

The force curves agree with the experimental observations. The results for Scheme #3 verified that the two-loop coil design can provide vertical bulk-stability, but generally cannot provide horizontal bulk stability.

5.6 Summary

The experimental and analytical results for all three schemes are summarized in Table 5-1. The abbreviations V.B.S. and H.B.S. refer to vertical bulk stability and horizontal bulk stability of the system. In Scheme #1, a range of levitation heights exist in which the system

has both vertical and horizontal bulk stability. However this range is approximately 3 mm, and is too small for practical purposes. In Scheme #2, the system does not have horizontal bulk stability. This result is contrary to the infinite-cylinder analysis from [1]. Increasing the radius ratio from 5:1 to 20:1 does not improve the horizontal bulk stability. In Scheme #3, stable levitation was only possible when the load was tethered to the centre of the coil. The results show that the two-loop coil is not capable of stably levitating a torus, primarily because this system lacks horizontal bulk stability.

Scheme #	Experimental Results	Regions of V.B.S.	Regions of H.B.S.
1	Unstable	h>17mm	H<20mm D<10mm
2	Unstable	h>15mm	None
3	Stable, as long as load is teathered	all h	None

Table 5-1, Summary of results for two-loop schemes

CHAPTER 6
LEVITATION USING A REVERSE-LOOP

6.1 Introduction

In Chapter 5, the levitation of a load using a two-loop induction coil was discussed. The general result was that stable levitation was not possible with this design. This was largely due to a lack of horizontal bulk stability. The strategy for overcoming this problem was to copy the practice of the traditional spherical levitation device. As mentioned in Chapter 1, this device consists of two sets of coils. The lower set provides most of the lifting force, while the upper set provides horizontal bulk stability. The upper set and lower set are wound in opposite directions. For this reason, the upper set is sometimes called a "reverse-loop". Three different reverse-loop schemes are examined in this chapter.

6.2 Scheme #1

The first scheme to implement this strategy is shown in Figure 6-1. The induction coil consisted of two lifting loops and one reverse-loop. The flat ring was used as the load. The separation height h_s between the lifting loops and reverse loop could be adjusted from 1 cm to 3 cm.

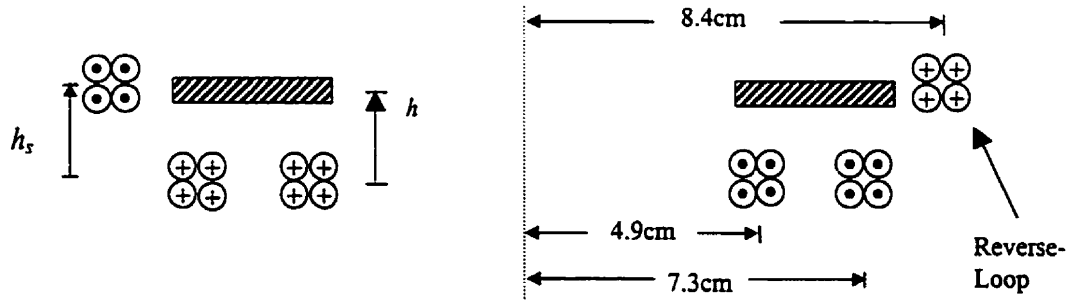

Figure 6-1, Reverse-Loop Scheme #1

Experiments

Trials were done using different values of h_s. At certain separation heights, the load levitated stably about 1 or 2 cm above the coil (Figure 6-2). The load did not make contact

with any part of the coil. Small horizontal oscillations were observed, but the system had both vertical and horizontal bulk stability. The stability was strongly dependent on the position of the reverse loop. For example, if h_s was too large, the load would move horizontally and slide into the gap between the outer lifting loop and the reverse loop. Also, if the reverse loop was not coplanar with the two lifting loops, this had an adverse effect on the bulk stability of the system. The reverse-loop had to be positioned by trial and error in order to find a bulk-stable configuration. In spite of this difficulty, the experiments on this scheme showed the usefulness of the reverse-loop design in providing horizontal bulk stability.

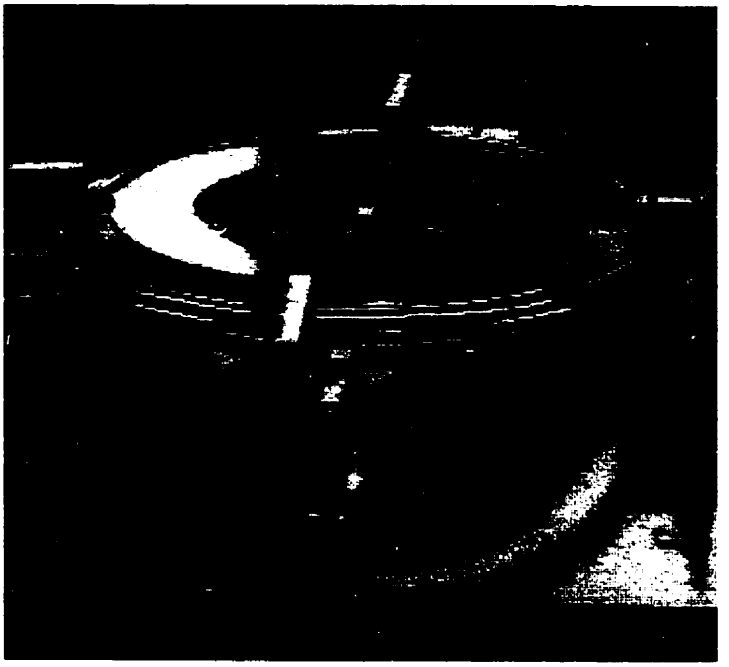

Figure 6-2, Picture of Levitating Flat Ring for
Reverse-Loop Scheme #1

Analysis

Two different values of h_s were considered in the analysis of Scheme #1. The first analysis used a separation height of 1.2 cm. Figure 6-3 shows a plot of the magnetic field streamlines for this case.

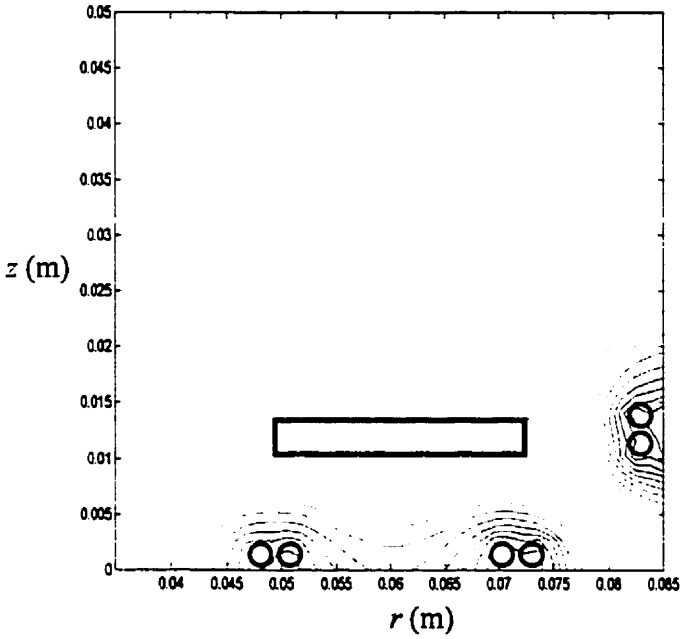

Figure 6-3, Streamline plot for Reverse-Loop Scheme #1 with h_s =1.2 cm

Figure 6-4 shows a plot of the vertical force curve. The slope is always negative, and vertical bulk stability can be achieved at all levitation heights.

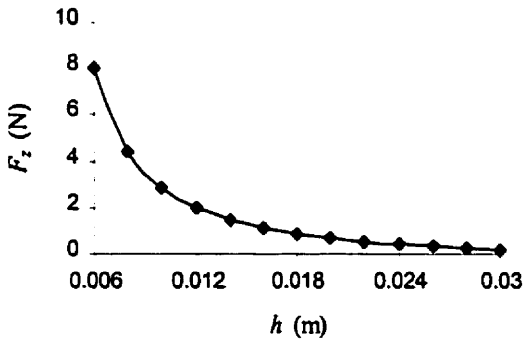

Figure 6-4, Vertical force curve for Reverse-Loop Scheme #1 with h_s =1.2 cm

Figure 6-5 shows a plot of the horizontal force curves. The curves were plotted for three levitation heights in the vicinity of h_s: 0.8 cm, 1.0 cm and 1.2 cm. For each curve, the slope is positive near the origin, and the system does not have horizontal bulk stability.

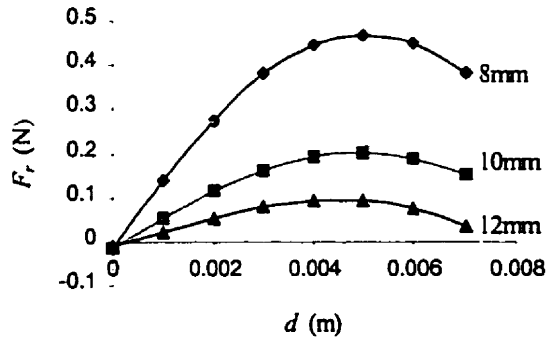

Figure 6-5, Horizontal force curve for Reverse-Loop Scheme #1 with h_s =1.2 cm

In the second analysis, the separation height was changed to 2.0 cm. Figure 6-6 shows the streamline plot for this case.

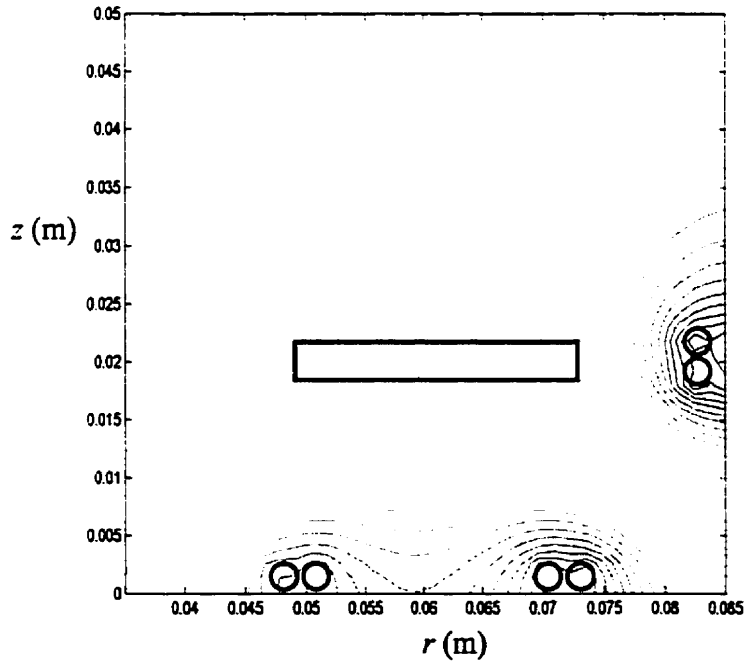

Figure 6-6, Streamline plot for Reverse-Loop Scheme #1, with h_s = 2.0 cm

The vertical force curve is shown in Figure 6-7. It does not differ significantly from the curve for h_s = 1.2 cm. The slope is always negative, indicating that vertical bulk stability can be achieved at any height.

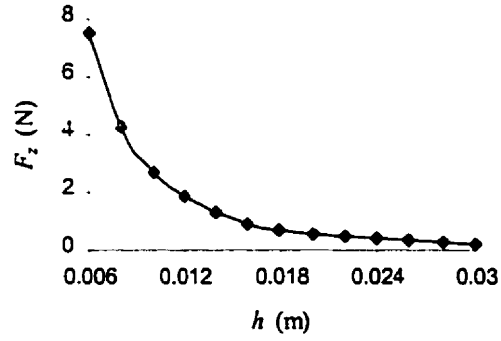

Figure 6-7, Plot of vertical force curve for Reverse-Loop Scheme #1 with h_s =2.0 cm

Figure 6-8 shows a plot of the horizontal force curves when h_s = 2.0 cm. The force curve was plotted at three different levitation heights: 15 mm, 20 mm and 25 mm. At 20 mm and 25 mm, there is no problem with the horizontal bulk stability, as the force curves are negatively sloped near the origin. However, for h = 15 mm, the force curve is positively sloped, and the system does not have horizontal bulk stability.

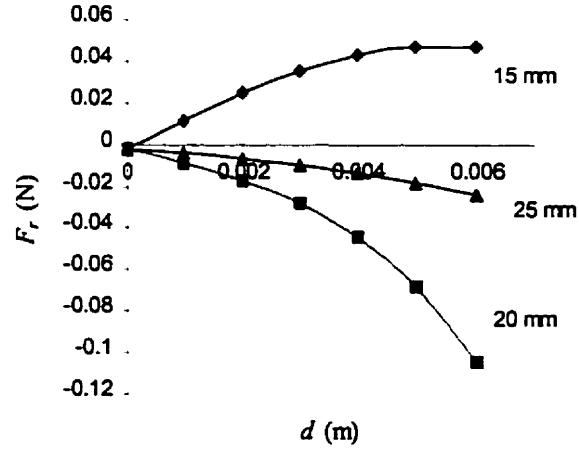

Figure 6-8, Horizontal force curves for Reverse-Loop Scheme #1, with h_s =2.0 cm

The analytical force curves agree with the experimental observations. The results show that stable levitation is possible at certain levitation heights and for particular values of h_s. The analysis also illustrates how the bulk stability of the system is strongly affected by changes in the position of the reverse loop. A change of 8 mm in the separation height makes the difference between a stable system and an unstable system.

The streamline plots for Scheme #1 show that there is a point on the surface of the load where the magnetic pressure is zero. This occurs on the lower outside edge of the load, where the streamlines are not tangential to the surface. The magnetic pressure distribution is plotted in Figure 6-9. The pressure is plotted on the edge of each of the 94 elements used to model the surface of the load, the first element being located on the upper outside edge of the load. The plot shows that there are regions on the top and bottom surfaces of the load where the magnetic pressure is zero (Figure 6-10). Although this scheme provides bulk stability, it does not provide a suitable magnetic pressure distribution for containing liquid metal.

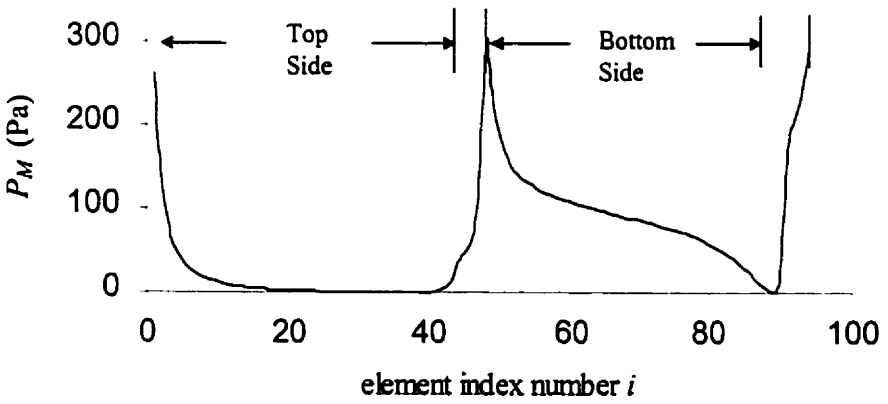

Figure 6-9, Pressure Distribution on Load
for Reverse-Loop Scheme #1

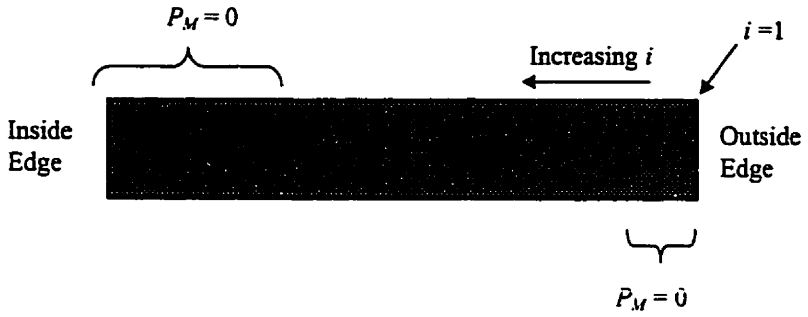

Figure 6-10, Regions where $P_M = 0$

6.3 Scheme #2

A second reverse-loop scheme was built to levitate the torus. The scheme is characterized by two lifting loops and two reverse-loops (Figure 6-11).

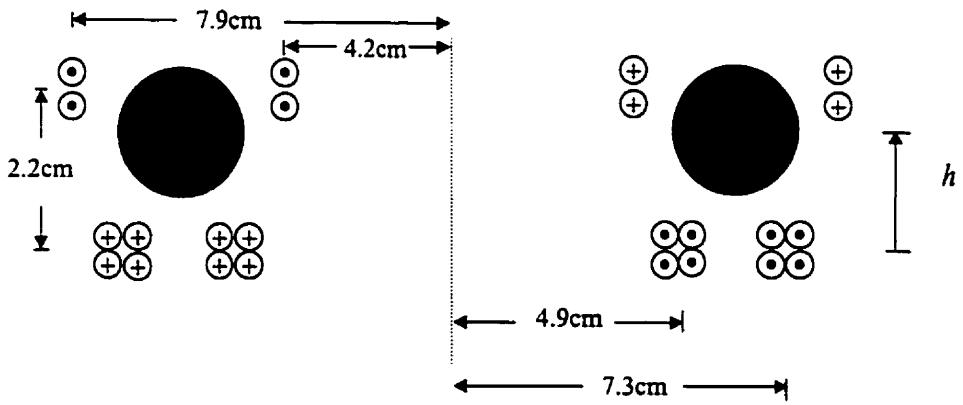

Figure 6-11, Reverse-Loop Scheme #2

Experiment

When the coil was energized, the torus levitated at a height of approximately 2 cm (Figures 6-12 and 6-13). There was very little horizontal motion, indicating that the system had horizontal bulk stability. However, the load experienced undamped oscillations in the vertical direction. The amplitude of oscillation was approximately 0.4 cm, and the frequency was approximately 4 Hz. External mechanical forces were applied to damp the oscillations.

When the oscillations were completely damped, the load continued to levitate without oscillating for about 2 or 3 seconds. This indicated that the system had vertical bulk stability to some extent. However, small oscillations started to develop after 3 seconds, and the oscillation amplitude grew to a maximum within approximately 10 seconds.

Figure 6-12, First picture of levitating torus for Reverse-Loop Scheme #2

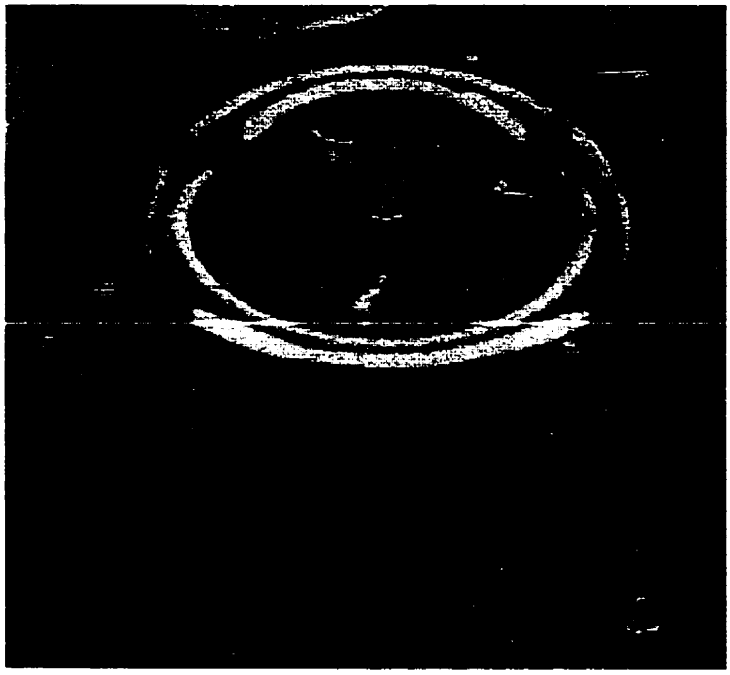

Figure 6-13, Second picture of levitating torus for
Reverse-Loop Scheme #2

Analysis

Figure 6-14 shows a plot of the magnetic field streamlines for Scheme #2. There are two locations on the surface of the load where the magnetic pressure is zero. This is verified by a plot of the magnetic pressure distribution, shown in Figure 6-15. The hydrostatic pressure distribution is also plotted on the graph for comparison. Ideally, the two distributions should match, but the plot shows that this is not the case. This scheme is not ideal for levitating a molten torus, as there are magnetic holes through which the molten metal can leak.

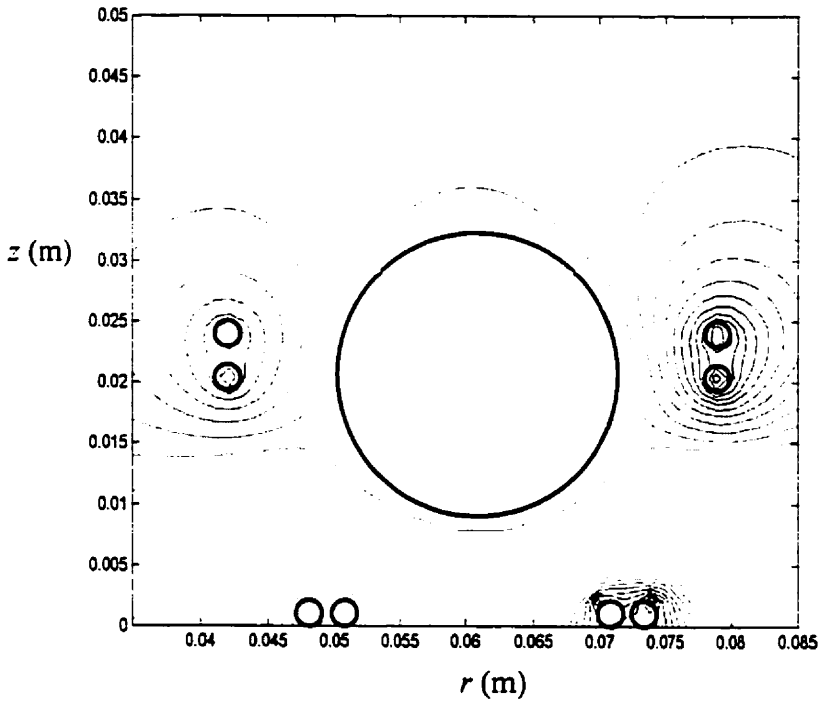

Figure 6-14, Streamline plot for Reverse-Loop Scheme #2

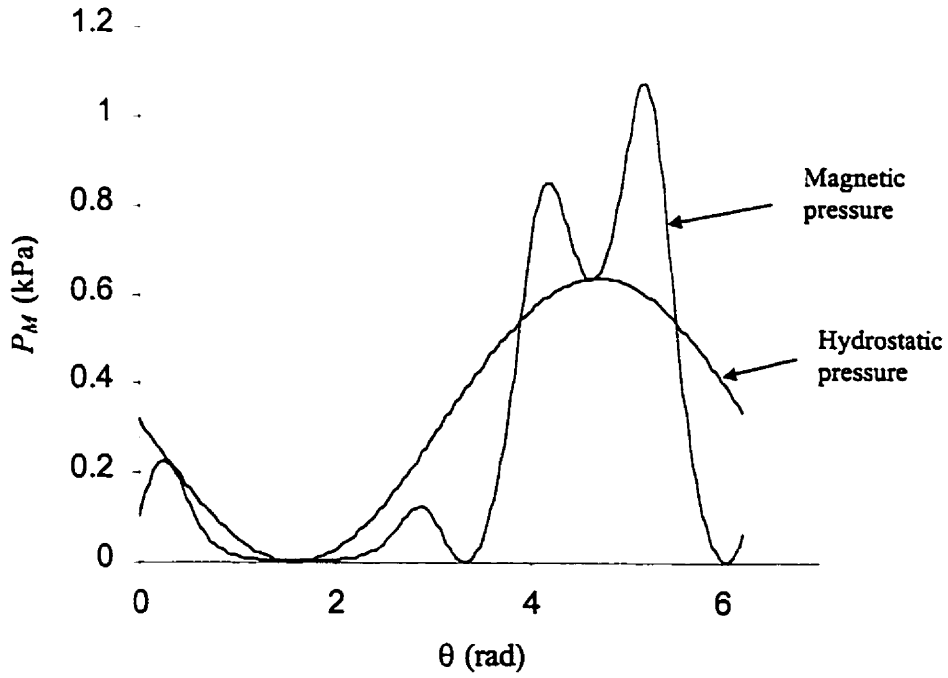

Figure 6-15, Magnetic pressure distribution for Reverse-Loop Scheme #2

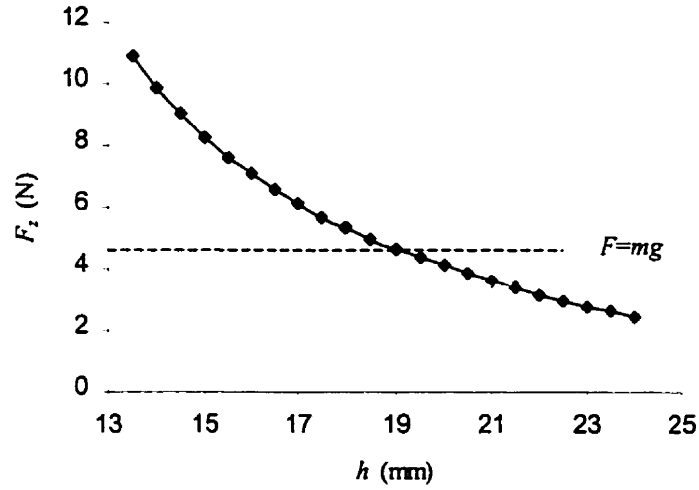

Figure 6-16, Vertical force curve for Reverse-Loop Scheme #2

Figure 6-16 shows a plot of the vertical force curve. The slope is always negative, indicating that the system has vertical bulk stability at all heights. Figure 6-17 shows a plot of the horizontal force curves. The force curves were plotted for three different levitation heights: 16 mm, 19 mm and 22 mm. At all three heights, the slope of the force curve is negative for radial displacements up to 6mm, indicating that the system has horizontal bulk stability within this range.

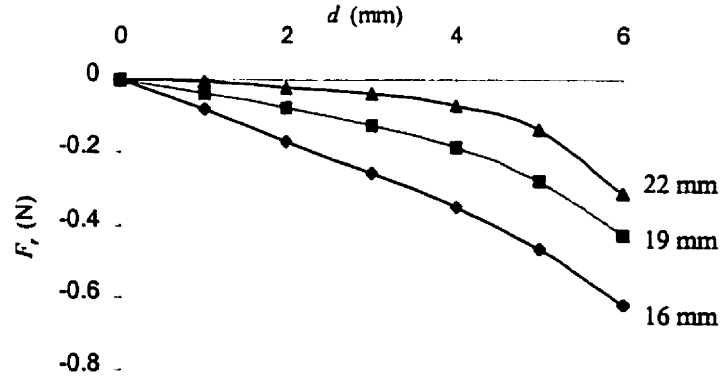

Figure 6-17, Horizontal force curve for Reverse-Loop Scheme #2

During the experiments, vertical undamped oscillations of the load were observed. It was desired to model the load oscillations and relate the results to the experimental observations. The first attempt to model the vertical oscillations considered only small displacements about the equilibrium position. This restriction simplifies the analysis, because the vertical force curve can be approximated by a first-order Taylor expansion about the equilibrium position. The essential parameter in the approximation is α, which is the slope of the vertical force curve at the equilibrium height h_{eq}. From Figure 6-16, the vertical force equals the weight of the torus (4.7 N) at a height of 19 mm. This is approximately the equilibrium levitation height observed during experiments. The slope of the curve at this point was calculated to be -610 N/m. The vertical oscillation frequency can be calculated using Equation 3.39:

$$\omega_z = \sqrt{\frac{-\alpha}{m}}$$

where m is the mass of the load (0.47 kg). The resulting oscillation frequency is 5.7 Hz. This is in the neighborhood of the oscillation frequency of 4 Hz observed in the experiments.

The linearization of the force curve is suitable for displacements approximately 3 mm above and below h_{eq}. For displacements beyond this range, the non-linear nature of the curve must be considered. This was done by approximating the vertical force curve as a third order polynomial of the form:

$$F_z = a_o + b_o h + c_o h^2 + d_o h^3 \qquad (6.1)$$

where a_o, b_o, c_o, and d_o are constants obtained through curve-fitting. The Runge-Kutta method (from Boyce et al. [25]) was used to solve the resulting non-linear differential equation of motion.

Figure 6-18 shows two curves representing the vertical motion of the load. The first curve, $H_1(t)$ is the result of a linear analysis, with the initial conditions h_o = 21 mm and $\dot{h}_o$ = 0. The second curve, $H_2(t)$ is the result of the non-linear analysis, and used the initial conditions h_o = 14 mm and $\dot{h}_o$ = 0. The curves have two common features: the frequency is the same, and the amplitude of oscillation does not decay with time.

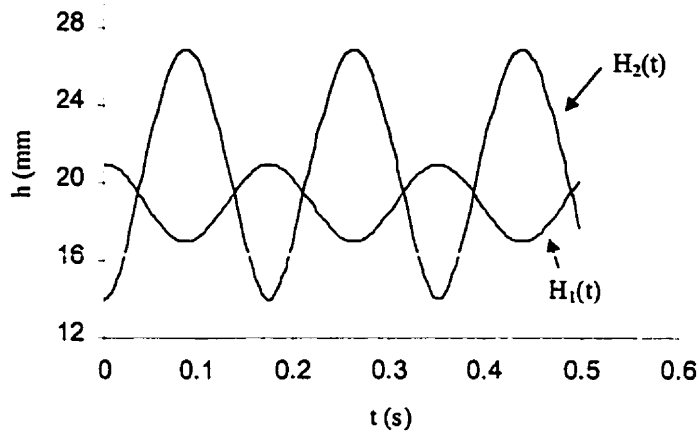

Figure 6-18, Plot of vertical oscillations for Reverse-Loop Scheme #2

In spite of the fact that mechanical modeling predicts an oscillation frequency similar to that observed in experiments, the model does not explain what causes the oscillations. The vertical oscillations appeared to develop naturally in the experiments, as there were no obvious physical disturbances acting on the load. This contradicts the results of the mechanical model. According to the model, if the load is not displaced from the equilibrium position, then it will remain at the equilibrium position indefinitely.

Essman et al. [16] encountered similar stability problems in the levitation of a spherical load. They concluded that modulations in the power supply signal must be eliminated in order to guarantee bulk stability of the system. It is possible that the same problem existed in the experiments for this thesis. The frequency was read from a digital display on the inverter. During one experiment, the excitation frequency was observed to fluctuate between 14.9 and 15.1 kHz, showing that there were modulations. Thus, the source of the vertical oscillations observed in this thesis might possibly be related to the power supply.

6.4 Scheme #3

In the third scheme, extra turns were added to the reverse loops of the four-loop coil, as shown in Figure 6-19. The purpose was to see what effect the number of reverse loops had on the behavior of the levitation system.

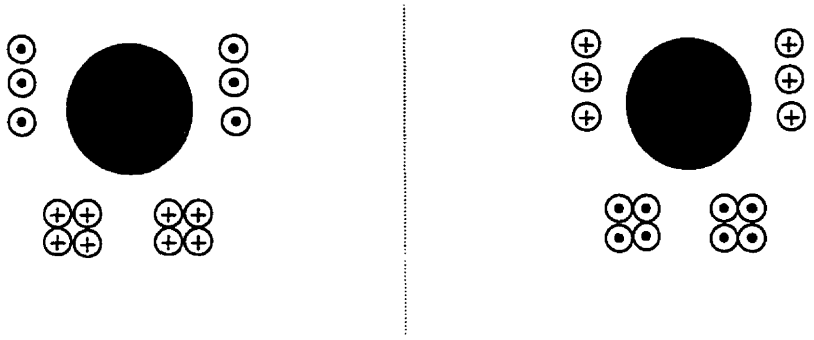

Figure 6-19, Reverse-Loop Scheme #3

Experiments

When the coil was energized, the load levitated stably. The levitation height was reduced to about 15mm. The load experienced small oscillations, primarily in the vertical direction. The oscillation frequency was approximately 4-5 Hz, and the amplitude of oscillation was 1-2 mm.

Analysis

The streamline plot for Scheme #3 is shown in Figure 6-20. The plot is similar to Scheme #2, showing two places on the surface where the magnetic pressure is zero. The vertical force curve for Scheme #3 is shown in Figure 6-21. It looks very similar to that for Scheme #2, and it is clear that the system has vertical bulk stability for all levitation heights. Figure 6-22 shows the horizontal force plot. The slopes of the curves are consistently negative, indicating that the system also has horizontal bulk stability.

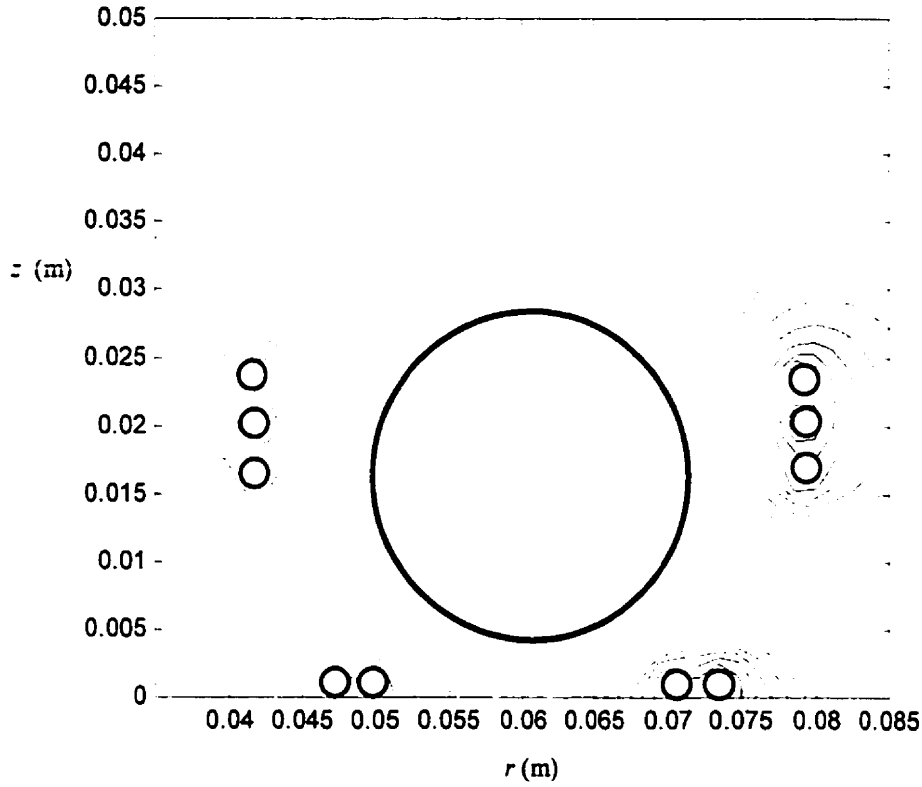

Figure 6-20, Streamline plot for Reverse-Loop Scheme #3

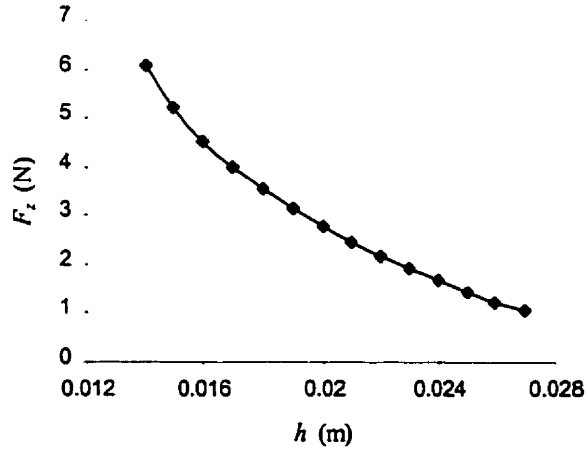

Figure 6-21, Vertical force curve for Reverse-Loop Scheme #3.

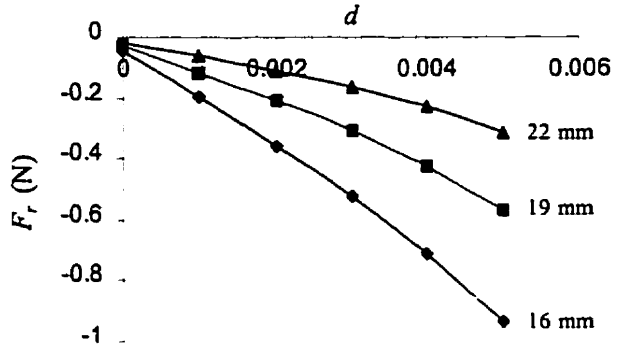

Figure 6-22, Horizontal force curves for Reverse-Loop Scheme #3.

6.5 Summary

The results for the reverse-loop coils are summarized in Table 6-1. The experiments with the reverse loop coils showed that this design is effective in providing vertical and horizontal bulk stability. It represents an improvement upon the two-loop coil design studied in the previous chapter. However, the analyses of the three schemes revealed one common problem: there are magnetic holes present on the surface of the load. This makes the design undesirable for levitating molten loads.

Scheme	Experimental Results	Analysis Results		
		V.B.S	H.B.S.	Pressure Distribution
1	Bulk stable, with a Strong dependence on reverse-loop position	All h	Hs=20mm h=20-25mm d<6mm	Undesirable
2	Bulk stable, but load tends to oscillate in vertical direction	All h	h=16-22mm d<6mm	Undesirable
3	Bulk stable, reduced levitation height, and reduced oscillation amplitude.	All h	h=16-22mm d<5mm	Undesirable

Table 6-1, Summary of results for reverse-loop schemes

CHAPTER 7
LEVITATION USING A BASKET COIL DESIGN

7.1 Introduction

The experiments on the reverse-loop coil designs showed that bulk-stability could be achieved with this design. However, the analysis showed that these designs do not provide a desirable pressure distribution on the surface of the load. Magnetic holes exist on the lower surface, making the reverse-loop designs unsuitable for containing large amounts of molten metal. A third coil design was constructed to try and rectify this problem. The design was referred to as the 'basket coil'. The idea was to surround the torus with a basket of loops, as shown in Figure 7-1. The induction coil consisted of 15 loops, all wound in the same direction. The locations of the conductors are equally spread out on a semi-circular arc.

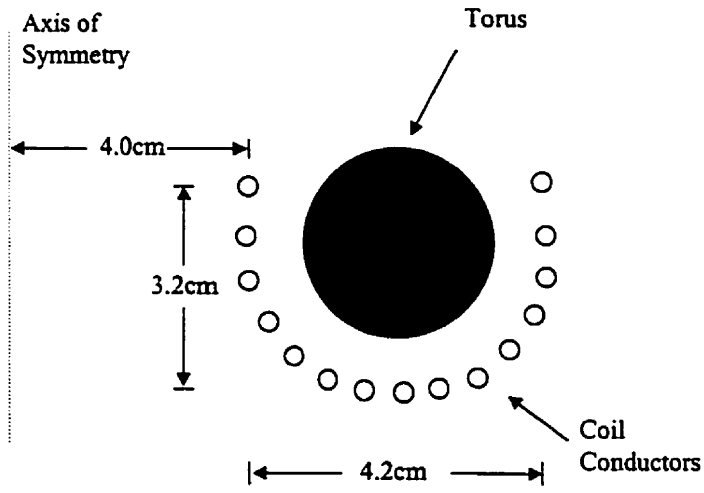

Figure 7-1, Basket Coil Design

7.2 Experiments

Initial attempts to levitate the torus were unsuccessful. It was believed that the self inductance of the coil was too large for the system to operate properly. The self inductance of the coil is approximately proportional to the square of the number of loops. The basket coil

consisted of 15 loops, and therefore had a relatively large inductance compared to the previous coils. The circuit could not be properly tuned, as the resonant frequency of the circuit was below the operating range of the inverter. It was decided to place an inductor L_p in parallel with the induction coil, as shown in Figure 7-2. This reduced the equivalent inductance of the load, raised the resonant frequency of the circuit, and allowed the inverter to operate properly.

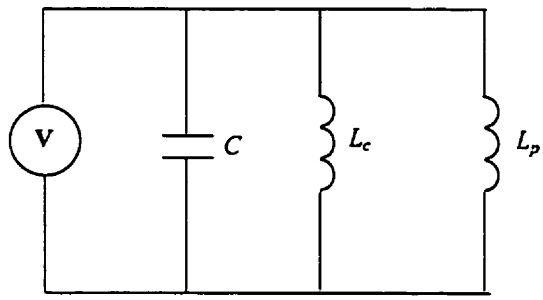

Figure 7-2, Equivalent circuit with an inductor connected in parallel with the induction coil

When the maximum voltage was applied to the modified circuit, one side of the torus levitated, while the opposite side remained resting on the induction coil. This behavior was similar to that observed during experiments with the first two-loop scheme. This might suggest that the basket design does not have bulk stability. However, levitation may have been inhibited by the limitations of the available power supply. It is possible that the inverter could not supply a sufficient output voltage to the induction coil. Bulk stable levitation may or may not be possible with this system, but this could not be determined from the experiments.

7.3 Analysis

In the analysis of the basket coil design, it was assumed that a sufficient power supply (with no limitations on applied output voltage) was used to energize the induction coil. The experimental results were inconclusive because of the power supply limitations. The results

of the analysis may be used to predict what would happen if a sufficient power supply was available for the experiments. Figure 7-3 shows a plot of the magnetic field streamlines for the basket coil, with the load levitating at a height of 2 cm. There is a noticeable difference between this plot and the streamline plots for the reverse-loop coils. There is no evidence of a magnetic hole anywhere on the surface of the load. This is verified by the plot of magnetic pressure distribution in Figure 7-4. The hydrostatic pressure distribution is also plotted for comparison.

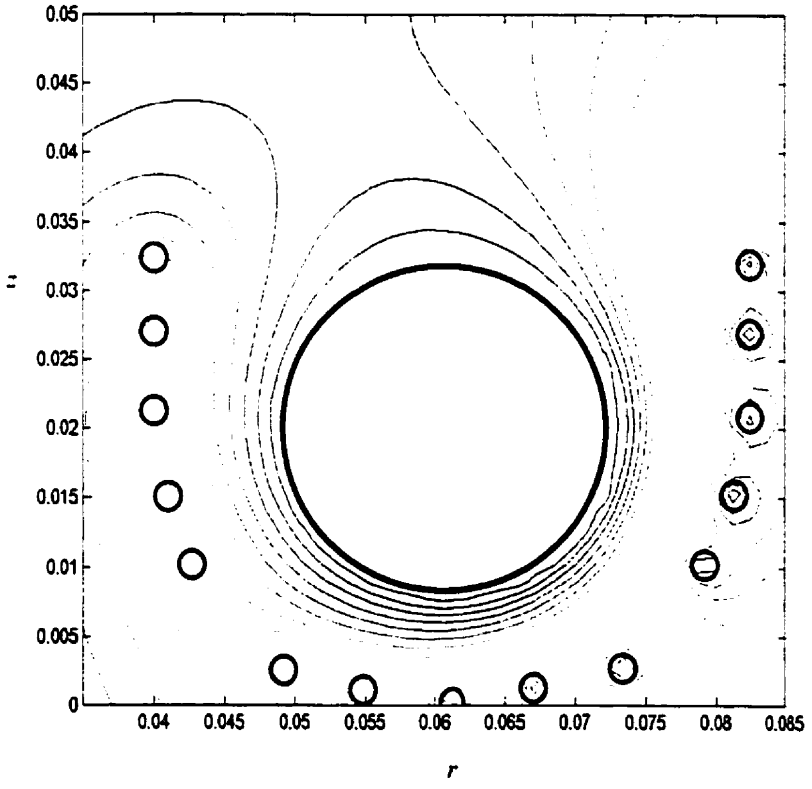

Figure 7-3, Streamline plot for the basket coil

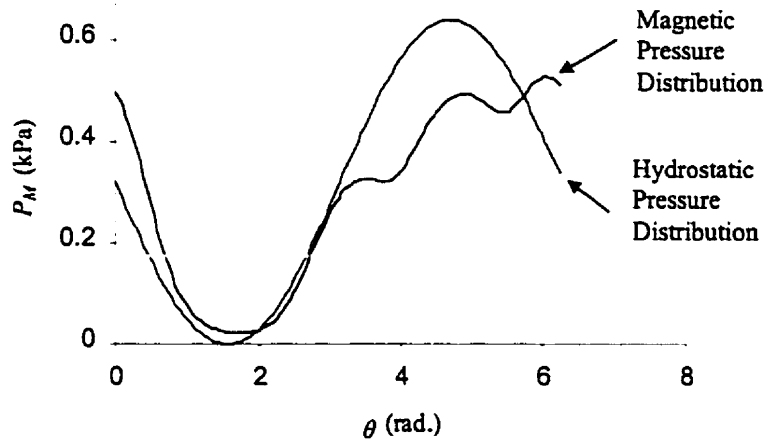

Figure 7-4, Pressure distribution for the basket coil

Figure 7-5 shows a plot of the vertical force curve. The curve is almost linear over the range of levitation heights between 14 mm and 40 mm. The slope is always negative, indicating that vertical bulk stability is possible at all heights.

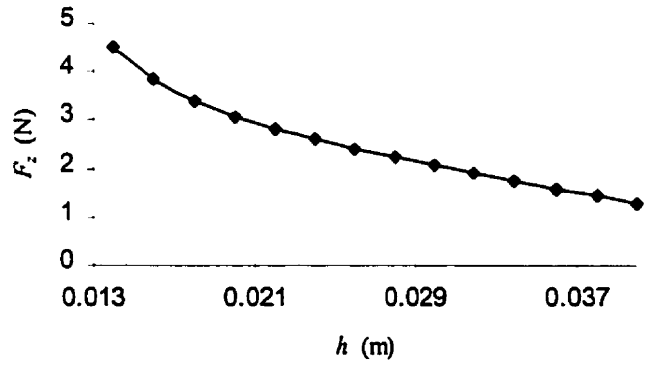

Figure 7-5, Vertical force curve for the basket coil.

Figure 7-6 shows a plot of the horizontal force curves. The curves are plotted for levitation heights of 20 mm, 25 mm and 30 mm, and for displacements up to 7 mm. The slopes of the

curves are negative at all three heights, indicating that the system has horizontal bulk stability.

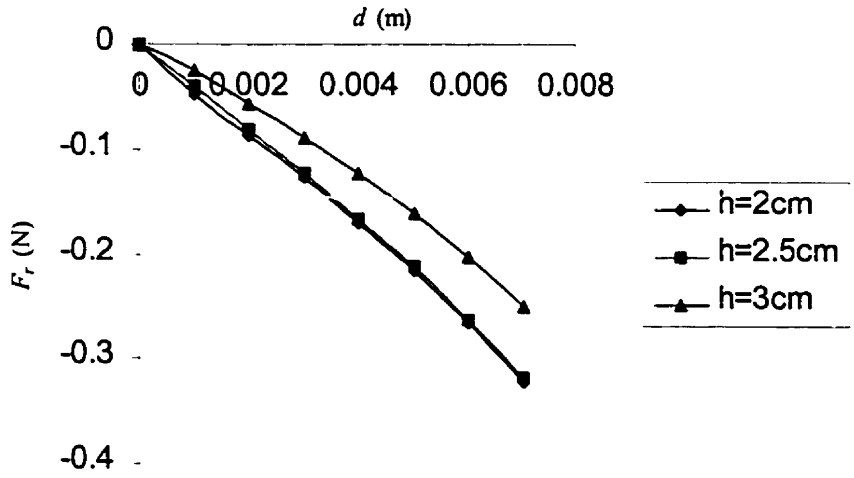

Figure 7-6, Plot of horizontal force curves for the basket coil

The analysis shows that this particular basket-coil design has both vertical and horizontal stability. In addition, the magnetic pressure distribution is suitable for levitating liquid metals, as there are no magnetic holes on the surface of the load. Therefore, the basket coil design holds much potential for increasing the amount of molten metal in the levitation melting process.

The magnetic pressure distribution differs slightly from the hydrostatic pressure distribution. The differences between the two distributions are due to the fact that the coil has not been optimized. It was initially decided to have the conductors of the coil equally spaced for the sake of simplicity. However, it is possible to reduce the error by relocating the conductors. This procedure was discussed by Bendzsak [21]. In his work, a ten-loop basket coil was optimized for containing a molten torus. He obtained a coil design whose pressure distribution closely matches the hydrostatic pressure distribution.

7.4 Fluid Flow in the Molten Torus

It was decided to obtain a qualitative description of the flow patterns that would develop in the molten toroidal load. Several numerical methods may be used to solve this flow problem. However, it was decided to adopt the analytical method used by Sneyd et al.[1] to determine the cross-sectional flow pattern in a molten infinite cylinder. The toroidal curvature of the load is not taken into account.

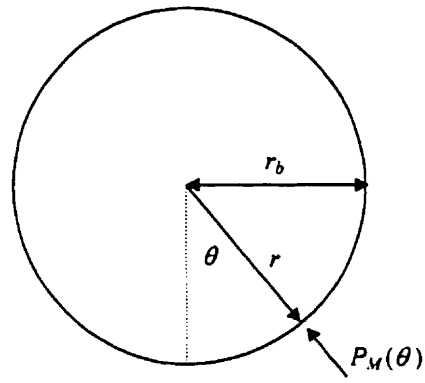

Figure 7-7, Cross-section of cylindrical load

An ideal situation is considered, in which the magnetic pressure P_M balances the hydrostatic pressure at all points on the surface of the load. With reference to Figure 7-7, the magnetic pressure is given by the equation:

$$P_M = \rho g r_b (1 + \cos\theta) \qquad (7.1)$$

where ρ is the density of molten metal (2370 kg/m^3 for Aluminum), g is the acceleration of gravity (9.81 m/s^2), and r_b is the cross-sectional radius of the load (0.012 m).

The flow in the molten load is likely to be turbulent. The Reynolds number R_e is given by the equation:

$$R_e = \frac{u_o L}{\nu} \qquad (7.2)$$

where u_o is the characteristic velocity of the fluid, L is the characteristic dimension of the load (equal to $2r_b$) and ν is the kinematic viscosity of the molten metal. In [1], Sneyd and Moffatt

argue that the flow is likely to be turbulent for $L \geq 10$ mm. It is also argued that turbulence limits the level of internal fluid velocity to the free fall scale, such that:

$$u_o \sim \sqrt{gL} \tag{7.3}$$

A uniform eddy viscosity $\nu_T \sim u_o L$ is assumed throughout the fluid, so that the corresponding Reynolds number is on the order of unity. Therefore, a low-Reynolds-number analysis is performed, in which the viscous forces are assumed to dominate over the inertial forces.

The momentum equation for fluid flow can be written as:

$$\left(\frac{\partial \mathbf{v}}{\partial t} + \mathbf{v} \cdot \nabla \mathbf{v}\right) = -\frac{\nabla p}{\rho} + \mathbf{g} + \frac{\mathbf{f}_L}{\rho} + \nu_T \nabla^2 \mathbf{v} \tag{7.4}$$

where ρ is the density, $\mathbf{v}$ is the velocity vector, p is the pressure, $\mathbf{g}$ is the acceleration of gravity, and $\mathbf{f}_L$ is the Lorentz force. The left hand side of Equation 7.4 is zero, because the problem is solved for steady-state flow and the convection term is neglected. Equation 7.4 can be rewritten as:

$$\nu_T \nabla^2 \mathbf{v} = \frac{\nabla p}{\rho} - \mathbf{g} - \frac{\mathbf{f}_L}{\rho} \tag{7.5}$$

Taking the curl of both sides of Equation 7.5 results in:

$$\nabla^2 \omega = -\frac{1}{\rho \nu_T} \nabla \times \mathbf{f}_L \tag{7.6}$$

ω is the vorticity, which is defined as the curl of the velocity vector. The vorticity has only one component ω_ζ in the ζ direction, perpendicular to the r-θ plane. This is related to the streamfunction by:

$$\omega_\zeta = \nabla^2 \psi \tag{7.7}$$

Boundary layer methods from [1] show that the curl of the Lorentz force is:

$$\nabla \times \mathbf{f}_L = -\frac{2}{\delta}(\hat{\mathbf{n}} \times \nabla P_M) \exp\left[-\frac{2(r_b - r)}{\delta}\right] \tag{7.8}$$

where $\hat{\mathbf{n}}$ is the inward normal unit vector on the surface of the load. After substituting Equations 7.7 and 7.8 into Equation 7.6, it can be shown that the streamfunction satisfies the inhomogeneous bi-harmonic equation:

$$\nabla^4\psi = \frac{2g}{\nu_T\delta}\exp\left(\frac{-2(r_b - r)}{\delta}\right)\sin\theta \tag{7.9}$$

where δ is the electromagnetic penetration depth (0.06 cm).

The surface of the load (where $r = r_b$) is a streamline, specified by the boundary condition ψ=0. A second boundary condition is imposed by the fact that the tangential stress is zero on the free surface. The tangential stress is:

$$\tau_{r\theta} = \rho\nu_T\left(\frac{\partial v_\theta}{\partial r} - \frac{v_\theta}{r}\right) \tag{7.10}$$

The θ component of velocity is related to the derivative of the streamfunction.

$$v_\theta = \frac{\partial\psi}{\partial r} \tag{7.11}$$

Therefore, the second boundary condition is given by the expression:

$$\frac{\partial^2\psi}{\partial r^2} - \frac{1}{r}\frac{\partial\psi}{\partial r} = 0, r = r_b \tag{7.12}$$

It can be shown (from Equation 6.5 in [1]) that the approximate solution for ψ is:

$$\psi(r,\theta) = \frac{g{r_b}^2\delta}{8\nu_T}\left(1 - \left(\frac{r}{r_b}\right)^2\right)\frac{r}{r_b}\sin\theta \tag{7.13}$$

The flow pattern can be illustrated by plotting the contour lines of the streamfunction $\psi(r,\theta)$. Figure 7-8 shows a plot of the streamlines. The flow is symmetric about the vertical axis of symmetry. There are two circulation patterns that occur within the load. It is reasonable to assume that in the actual torus, the flow would not be symmetric due to the toroidal curvature.

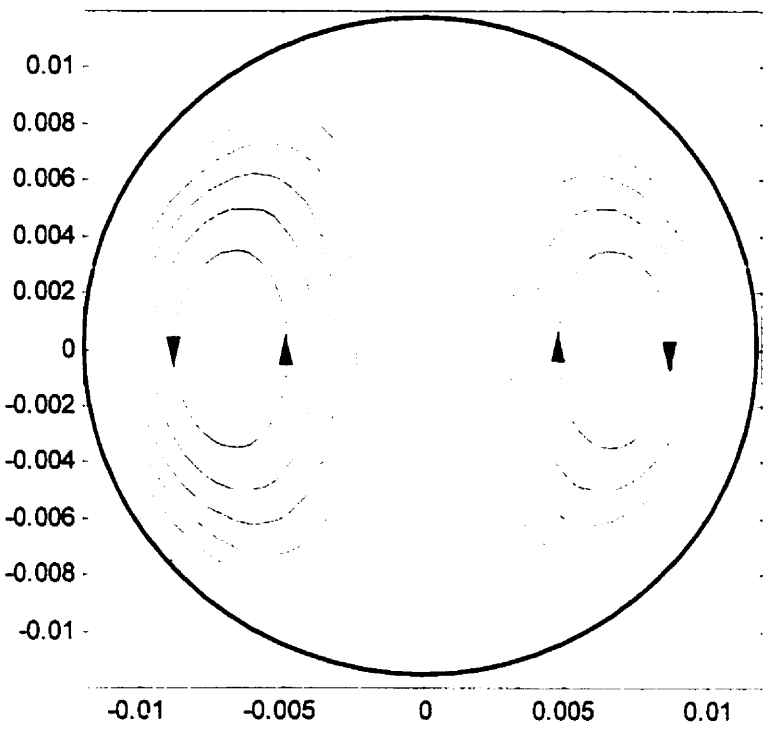

Figure 7-8, Plot of flow streamlines in the molten load

The fluid velocity can be obtained by differentiating the streamfunction. The surface velocity is given by the expression:

$$V_s = \left.\frac{\partial \psi}{\partial r}\right|_{r=r_b} \tag{7.14}$$

It can be shown that the resulting expression for surface velocity is:

$$V_s(\theta) = -\frac{g r_b \delta \sin\theta}{4\nu_T} \tag{7.15}$$

Figure 7-9 shows a plot of the surface velocity profile. The distribution is plotted for the right half of the load ($\theta = 0..\pi$) since the flow pattern is symmetric. The velocity reaches a peak value of approximately 1.7 mm/s at the mid-point, when $\theta = \pi/2$.

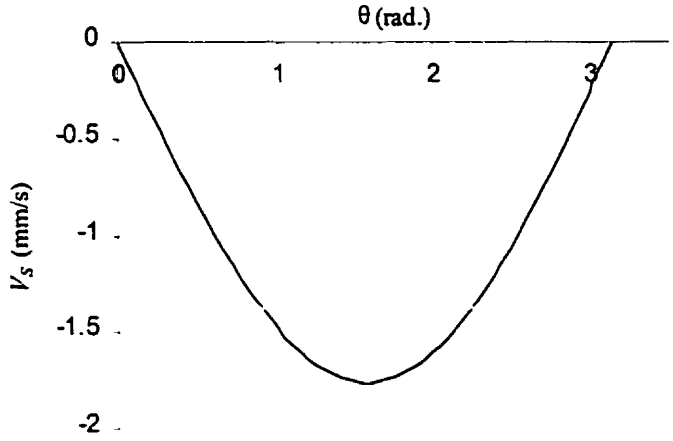

Figure 7-9, Plot of surface velocity profile

A plot of the velocity profile within the load is shown in Figure 7-10. The velocity is plotted along the line defined by $r = 0..r_b$ and $\theta = \pi/2$. Along this line, only the θ component of velocity (V_θ) exists. This is given by the expression:

$$V_\theta(r) = \frac{g r_b \delta}{8 \nu_T}\left[1 - 3\left(\frac{r}{r_b}\right)^2\right] \qquad (7.16)$$

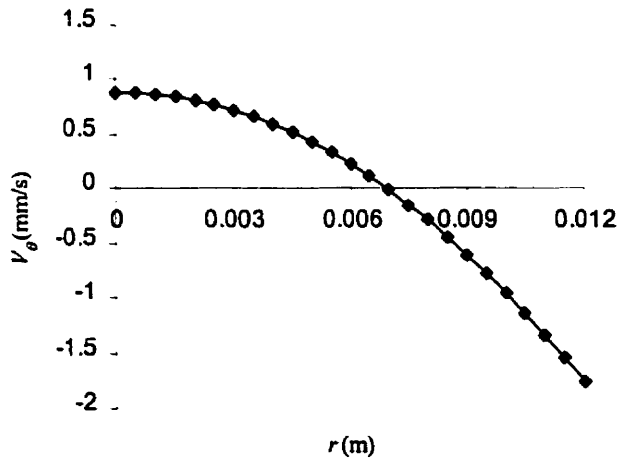

7-10, Plot of velocity profile within the load

7.5 Summary

The results of the analysis indicate that the basket coil design can provide both vertical and horizontal bulk stability. This result was not observed in the experiments, likely because of the limitations of the available power supply. The magnetic pressure distribution plot showed that there are no magnetic holes on the surface of the load, which makes this design suitable for levitating large amounts of molten metal. A simplified laminar flow analysis revealed that the cross-sectional flow pattern in the molten load is characterized by two recirculating loops. The analysis predicts that the fluid on the surface has a maximum velocity of approximately 1.7 mm/s.

CHAPTER 8
CONCLUSIONS

1) The two-loop coil designs (which were studied in this thesis) were determined to be unsuitable for levitating a solid toroidal load. In general, these designs suffer from a lack of horizontal bulk stability. It is possible to obtain vertical bulk stability alone with the two-loop coil; this was shown with the tethered-load experiment.

2) According to the infinite-cylinder analysis of [1], a stable levitation system can be realized by making the separation distance between the two loops equal to the cross-sectional diameter of the load (equivalent to setting κ=1). However, it was shown through experiments and analysis that this will not produce a bulk stable levitation system when the radius ratio r_a:r_b is approximately 5:1. This system did not have horizontal bulk stability.

3) It is to be expected that, as the radius ratio is increased, the results of a toroidal system should become closer to the infinite-cylinder system. An analysis was done for a toroidal system with an increased ratio of 20:1. This was also shown to be an unsuccessful system, as it did not have horizontal bulk stability.

4) The use of a reverse-loop is effective in providing horizontal bulk stability. Stable levitation was achieved for the three reverse-loop schemes considered in this thesis.

5) Experiments and analysis of Reverse-Loop Scheme #1 showed that the stability of the system is strongly dependent on the location of the reverse-loop. If the reverse-loop is not coplanar with the lifting loops, this has an adverse effect on the bulk stability of the system. A change by 8 mm in the height of the

reverse-loop makes the difference between a stable system and an unstable system.

6) The load experienced undamped harmonic oscillations during experiments on Reverse-Loop Scheme #2. These oscillations developed naturally after the load was brought to rest at the equilibrium levitation height. A simple mechanical model predicted an oscillation frequency in the neighborhood of the frequency observed in the experiments. However, the model could not explain the source of the oscillations. No obvious physical disturbances were present. The oscillations were most likely the result of modulations in the power supply voltage signal.

7) The addition of extra turns to the reverse-loops had the effect of lowering the levitation height and reducing the amplitude of oscillation of the load.

8) A common problem with the reverse-loop designs is that the magnetic pressure distribution does not balance the hydrostatic pressure distribution. There are magnetic holes on the surface of the load, through which molten metal can leak. Therefore, the reverse-loop design is not suitable for levitating large amounts of molten metal.

9) The available power supply was insufficient for energizing the basket coil directly. When the power supply was connected to the coil, the resonant frequency of the circuit was too low for the power supply to operate properly.

10) A parallel inductor was used to reduce the inductance of the circuit as perceived by the power supply. This raised the frequency of the circuit, and allowed the inverter to operate properly. In spite of this adjustment, stable levitation could not be achieved. It was believed that the inverter could not supply a sufficient output voltage to energize the induction coil.

11) The analysis of the basket coil design indicates that the system will have both vertical and horizontal bulk stability if an adequate power supply is used.

12) The pressure distribution for the basket coil design is an improvement on that for the reverse-loop design. No magnetic holes exist on the surface of the load. The analysis suggests that this design can satisfy the requirements of bulk stability and pressure distribution. It therefore holds much potential for increasing the amount of metal for the levitation melting process.

13) The simplified flow analysis revealed that the cross-sectional flow pattern in the molten torus is characterized by two recirculating loops. The analysis predicted that the flow velocity on the surface reaches a maximum value of 1.7 mm/s.

REFERENCES

1 A.D. Sneyd, H.K.Moffat, "Fluid dynamical aspects of the levitation-melting process", J. Fluid Mech., Vol. 117, pp. 45-70, 1982.

2 S.R. Sagardia, "Electromagnetic Levitation Melting of Large Conductive Loads", Ph.D. thesis, University of Toronto, 1974.

3 E.C. Okress, D.M. Wroughton, G. Comenetz, P.H. Brace, J.C.R. Kelly, "Electromagnetic Levitation of Solid and Molten Metals", J. Appl. Phy., Vol. 23, No. 5, pp. 545-552, 1952.

4 W.A. Peifer, "Levitation Melting, A Survey of the State-of-the-Art", J. Metals, Vol. 17, pp. 487-493, 1965.

5 A. Gagnoud, J.P. Brancher, "Modeling of Coupled Phenomena in Electromagnetic Levitation", IEEE Transactions on Magnetics, Vol. 21, No. 6, pp. 2424-2427, 1985.

6 N. El-Kaddah, J. Szekely, "The Electromagnetic Force Field, Fluid Flow Field, and Temperature Profiles in Levitated Metal Droplets", Metal. Trans. B, Vol. 14, pp. 401-410, 1983.

7 A.J. Mestel, "Magnetic levitation of liquid metals", J. Fluid Mech., Vol. 117, pp. 27-43, 1982.

8 M.R. Harris, S.Y. Stephan, "Support of liquid metal surface by alternating magnetic field", IEEE Transactions on Magnetics, Vol. Mag-11, No. 5, pp. 1508-1510, 1975.

9 S. Krishnan, G.P. Hansen, R.H. Hauge, J.L. Margrave, "Observations on the Dynamics of Electromagnetically Levitated Liquid Metals and Alloys at Elevated Temperatures", Metal. Trans. A, Vol. 19, pp. 1939-1943, 1988.

10 A. Kasama, A. McLean, W.A. Miller, Z. Morita, M.J. Ward, "Surface Tension of Liquid Iron and Iron-Oxygen Alloys", Can. Metall. Q., Vol. 22, No. 1, pp. 9-17, 1983.

11 W.B.Chung, K. Nogi, W.A. Miller, A.McLean, "Surface Tension of Liquid Cr-O Systems", Materials Transactions, JIM, Vol. 33, No. 8, 1992, pp. 753-757.

12 K.C. Mills, R.F. Brooks, "Measurements of thermophysical properties in high temperature melts", Materials Science and Engineering, A178, 1994, pp. 77-81.

13 W. Brisley, B.S. Thornton, "Electromagnetic levitation calculations for axially symmetric systems", Brit. J. Appl. Phys., Vol. 14, pp. 682-686, 1963.

14 A.J. Hatch, "Potential-Well Description of Electromagnetic Levitation", J. Appl. Phys., Vol. 36, No. 1, pp. 44-52, 1965.

15 L.M. Holmes, "Stability of magnetic levitation", J. Appl. Phys., Vol. 49, No. 6, pp. 3102-3109, 1978.

16 U. Essmann, H. Kiessig, "Preparation of Metals in Ultra High Vacuum by Electromagnetic Levitation", Mat. Res. Bull., Vol. 14, pp. 1139-1145, 1979.

17 A.V. Zhevnyak, D.P. Muzlov, "Stability of levitated conducting bodies in an axisymmetric electromagnetic field", Sov. Phys. Tech. Phys., Vol. 27, No. 7, pp. 790-792, 1982.

18 L.S. Piggot, G.F. Nix, "Electromagnetic levitation of a conducting cylinder", Proc. IEE, Vol. 113, No. 7, pp. 1229-1235, 1966.

19 A.P. Vutsens, "On the possibility of increasing the weight of a molten metal suspended in an electromagnetic crucible", Magnetohydrodynamics, No. 2, pp. 257-260, 1972.

20 A.P. Vutsens, "Freely levitating torus in the electromagnetic field of a current-carrying loop and a current-carrying axial conductor", Magnetohydrodynamics, Vol. 12, No. 4, pp 478-485, 1976.

21 G.J. Bendzsak, "An Algorithm for Solution of the Inverse Electromagnetic Liquid Metal Confinement Problem", Applied Computational Electromagnetics Society Journal, Vol. 11, No. 3, pp. 55-62, 1996.

22 S.L. Salas, E. Hille, "Calculus: one and several variables", 6th ed., John Wiley & Sons, Inc., 1990.

23 C. Kittel, W.D. Knight, M.A. Ruderman, "Mechanics", 2nd ed., McGraw-Hill, Inc., 1973.

24 J.D. Irwin, "Basic Engineering Circuit Analysis", 4th ed., Macmillan Publishing Company, 1993.

25 W.E. Boyce, R.C. DiPrima, "Elementary Differential Equations and Boundary Value Problems", 5th ed., John Wiley & Sons, Inc., 1992.

26 W. R. Smythe, "Static and Dynamic Electricity", 1st ed., McGraw-Hill, 1939.

27 K.B. Kim, E. Levi, Z. Zabar, L. Birenbaum, "Mutual Inductance of Noncoaxial Circular Coils with Constant Current Density", IEEE Trans. Magn., Vol. 33, No. 5, pp. 4303-4309, 1997.

28 E. Weber, "Electromagnetic Fields – Theory and Applications. Volume 1-Mapping of Fields", John Wiley & Sons, Inc., New York, 1950.

APPENDIX

A.1 Self Inductance of a Circular Filament Loop

It can be shown (see Smythe [26], for example) that the self-inductance L of a circular filament-loop is given by the expression:

$$L = \mu_o r_a \left[\ln\left(\frac{8r_a}{r_b}\right) - 2 \right] \qquad \text{(A.1)}$$

where r_a is the mean radius of the loop, and r_b is the cross-sectional radius of the conductor. This equation is accurate when r_a is significantly larger than r_b. The inductance is measured in units of Henrys.

A.2 Mutual Inductance Between Two Loops

Figure A-1 shows a diagram of two co-planar loops.

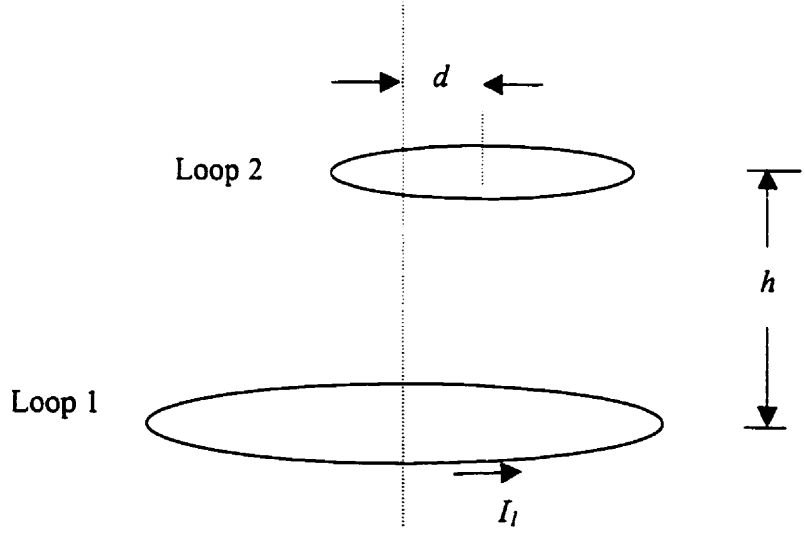

Figure A-1, Two coplanar loops

If the two loops are coaxial ($d = 0$), and separated by a distance h, the mutual-inductance between loops 1 and 2 is given by the formula:

$$M_{12} = \pm\frac{2\mu_o}{k}\sqrt{r_1 r_2}\left[\left(1 - \frac{k^2}{2}\right)K(k) - E(k)\right] \qquad \text{(A.2)}$$

where r_1 and r_2 are the radii of the two loops, K and E are the complete elliptic integrals of the first and second kind, respectively, and k is the elliptic integral parameter:

$$k = \sqrt{\frac{4r_1 r_2}{(r_1 + r_2)^2 + h^2}} \tag{A.3}$$

If there is some radial displacement d between the axes of the two loops, the mutual inductance can be determined (see Kim et al. [27]) using the formula:

$$M_{12} = \pm \frac{\mu_o r_2}{2\pi} \int_0^{2\pi} \frac{\sqrt{(r_1 + r_f)^2 + h^2}}{r_f} \cdot \left[\left(1 - \frac{k^2}{2} \right) K(k) - E(k) \right] \cdot d\phi \tag{A.4}$$

where

$$k = \sqrt{\frac{4r_1 r_f}{(r_1 + r_f)^2 + h^2}} \tag{A.5}$$

$$r_f = \sqrt{(r_2 \cos\phi + d)^2 + (r_2 \sin\phi)^2} \tag{A.6}$$

The mutual inductance is also measured in Henrys. The sign of the mutual inductance depends on whether the magnetic flux is additive or subtractive. If the current is defined as positive in the clockwise direction for both loops 1 and 2, then the magnetic flux adds, and the mutual inductance is positive. Otherwise, the mutual inductance is negative.

A.3 Details of the Coupled-Circuits Method

It was mentioned in Chapter 3 that the coupled-circuits method can be used to determine the current distribution on the surface of the levitating load. It was shown that the electromagnetic problem is described by the system of equations derived using Kirchoff's voltage law.

$$\{V\} = j\omega[M]\{I\} \tag{A.7}$$

where $\{V\}$ is the column vector representing the applied voltage to each element, $[M]$ is the inductance matrix, containing the self and mutual inductance terms, and $\{I\}$ is the column vector representing the current flowing through each element. In order to solve for the unknown currents {I} in the context of this thesis, some manipulation must be performed. The voltage vector $\{V\}$ can be broken up into two sub-vectors. Let $\{V_C\}$ represent the

applied voltage for each coil element. Let $\{V_L\}$ represent the applied voltage to each load element. Each load element is a short circuit, therefore all terms of $\{V_L\}$ are zero.

The same procedure can be followed for the current vector $\{I\}$. Let $\{I_C\}$ be the vector containing the current flowing through each coil element, and let $\{I_L\}$ be the vector containing the current flowing through each load element. All coil elements are connected in series, and therefore carry the same current $\mathbf{I_C}$.

In a similar fashion, the inductance matrix can be broken up into four sub-matrices:

$$[M]=\begin{bmatrix}[A] & [B]\\ [C] & [D]\end{bmatrix} \tag{A.8}$$

Rewriting Equation A.7 using the sub-vectors and sub-matrices results in

$$\begin{Bmatrix}V_C\\ V_L\end{Bmatrix}=j\omega\begin{bmatrix}[A] & [B]\\ [C] & [D]\end{bmatrix}\begin{Bmatrix}I_C\\ I_L\end{Bmatrix} \tag{A.9}$$

where

$$\{V_C\}_{m\times 1}=\begin{Bmatrix}V_1\\ V_2\\ \vdots\\ V_m\end{Bmatrix},\qquad \{V_L\}_{n\times 1}=\begin{Bmatrix}0\\ 0\\ \vdots\\ 0\end{Bmatrix},\qquad \{I_C\}_{m\times 1}=\mathbf{I_C}\begin{Bmatrix}1\\ 1\\ \vdots\\ 1\end{Bmatrix},\qquad \{I_L\}_{n\times 1}=\begin{Bmatrix}I_{m+1}\\ I_{m+2}\\ \vdots\\ I_p\end{Bmatrix},$$

$$[A]_{m\times m}=\begin{bmatrix}L_1 & M_{1,2} & \cdots & M_{1,m}\\ M_{2,1} & L_2 & \cdots & M_{2,m}\\ \vdots & \vdots & & \vdots\\ M_{m,1} & M_{m,2} & \cdots & L_m\end{bmatrix},\qquad [B]_{m\times n}=\begin{bmatrix}M_{1,m+1} & M_{1,m+2} & \cdots & M_{1,p}\\ M_{2,m+1} & M_{2,m+2} & \cdots & M_{2,p}\\ \vdots & \vdots & & \vdots\\ M_{m,m+1} & M_{m,m+2} & \cdots & M_{m,p}\end{bmatrix},$$

$$[C]_{n\times m}=[B]^T,\qquad [D]_{n\times n}=\begin{bmatrix}L_{m+1} & M_{m+1,m+2} & \cdots & M_{m+1,p}\\ M_{m+2,m+1} & L_{m+2} & \cdots & M_{m+2,p}\\ \vdots & \vdots & & \vdots\\ M_{p,m+1} & M_{p,m+2} & \cdots & L_p\end{bmatrix}$$

Two matrix equations can be written in terms of the unknown vectors $\{I_C\}$ and $\{I_L\}$:

$$\{V_C\}=j\omega\left([A]-[B][D]^{-1}[C]\right)\{I_C\}=j\omega[G]\{I_C\} \tag{A.10}$$

$$\{I_L\} = -[D]^{-1}[C]\{I_C\} \tag{A.11}$$

Since all terms of $\{I_C\}$ are identical, Equation A.7 can be further simplified to:

$$\{V_C\} = j\omega \mathbf{I}_C \{H\}_{m\times 1} \tag{A.12}$$

where the ith term of $\{H\}$ is the sum of all terms in the ith row of $[G]$.

The applied voltage to each element in the induction coil is not known. However the total voltage applied to the induction coil, **V**, is known. The sum of the applied voltages to each loop must equal **V**. Thus, for a given applied voltage **V**, the current flowing through the induction coil is:

$$\mathbf{I}_C = \frac{\mathbf{V}}{j\omega \sum_{i=1}^{m} H_i} \tag{A.13}$$

Once $\mathbf{I}_C$ is determined, the current distribution in the load may be determined using Equation 3.26.

A.4 Magnetic Flux Density and Magnetic Vector Potential

For a single, current carrying loop, the radial and axial components of the magnetic flux density vector **B** (measured in Webers per square meter) at a point in space q*(r,z)* may be determined using the equations (from Weber [28]):

$$B_r(r,z) = \frac{\mu_o I}{2\pi} \frac{z}{r\sqrt{(a+r)^2+z^2}} \left[-K(k) + \frac{a^2+r^2+z^2}{(a-r)^2+z^2} E(k) \right] \tag{A.14}$$

$$B_z(r,z) = \frac{\mu_o I}{2\pi} \frac{1}{\sqrt{(a+r)^2+z^2}} \left[K(k) + \frac{a^2-r^2-z^2}{(a-r)^2+z^2} E(k) \right] \tag{A.15}$$

where I is the current flowing in the loop, a is the radius of the loop, K and E are the complete elliptic integrals, and k is the elliptic integral parameter given by:

$$k = \sqrt{\frac{4ar}{(a+r)^2+z^2}} \tag{A.16}$$

The magnetic vector potential produced by a current carrying loop has only one component, which is in the angular or $\hat{\phi}$ direction. This can be determined using the formula:

$$A_\phi = \frac{\mu_o I}{2\pi r}\left[(r+a)^2 + z^2\right]^{1/2}\left[\left(1-\frac{k^2}{2}\right)K(k) - E(k)\right] \qquad \text{(A.17)}$$